https://doi.org/10.5194/hess-2022-377
Preprint. Discussion started: 21 November 2022
© Author(s) 2022. CC BY 4.0 License.

Hydrology and Earth System Sciences
Open Access
Discussions

Comparing machine learning and deep learning models for probabilistic post-processing of satellite precipitation-driven streamflow simulation

Yuhang Zhang[1], Aizhong Ye[1], Phu Nguyen[2], Bita Analui[2], Soroosh Sorooshian[2], Kuolin Hsu[2], Yuxuan Wang[3]

[1]State Key Laboratory of Earth Surface Processes and Resource Ecology, Faculty of Geographical Science, Beijing Normal University, Beijing 100875, China
[2]Center for Hydrometeorology and Remote Sensing, Department of Civil and Environmental Engineering, University of California, Irvine, Irvine, California, CA 92697, USA
[3]College of Arts and Sciences, University of Virginia, Charlottesville, Virginia, 22903, USA

Correspondence to: Aizhong Ye (azye@bnu.edu.cn)

Abstract. Deep learning (DL) models are popular but computationally expensive, machine learning (ML) models are old-fashioned but more efficient. Their differences in hydrological probabilistic post-processing are not clear at the moment. This study conducts a systematic model comparison between the quantile regression forest (QRF) model and probabilistic long short-term memory (PLSTM) model as hydrological probabilistic post-processors. Specifically, we compare these two models to deal with the biased streamflow simulation driven by three kinds of satellite precipitation products in 522 sub-basins of Yalong River basin of China. Model performance is comprehensively assessed by a series of scoring metrics from the probabilistic and deterministic perspectives, respectively. In general, the QRF model and the PLSTM model are comparable in terms of probabilistic prediction. Their performance is closely related to the flow accumulation area of the sub-basin. For sub-basins with flow accumulation area less than 60,000 km^2, the QRF model outperforms the PLSTM model in most of the sub-basins. For sub-basins with flow accumulation area larger than 60,000 km^2, the PLSTM model has an undebatable advantage. In terms of deterministic predictions, the PLSTM model should be more preferred than the QRF model, especially when the raw streamflow is poorly simulated and used as an input. But if we put aside the model performance, the QRF model is more efficient in all cases, saving half the time than the PLSTM model. This study can deepen our understanding of ML and DL models in hydrological post-processing and enable more appropriate model selection in practice.

Key words: Bias correction, long-short memory network, quantile regression forest, satellite precipitation, streamflow simulation.

https://doi.org/10.5194/hess-2022-377
Preprint. Discussion started: 21 November 2022
© Author(s) 2022. CC BY 4.0 License.

1 Introduction

By generalizing the physical processes, hydrologists or modelers abstract the hydrological mechanism into a series of numerical equations, which are collectively referred ~~to~~ as hydrological models (Sittner et al., 1969; Clark et al., 2015; Sivapalan, 2018; Chawanda et al., 2020; Zhou et al., 2021). Hydrological models are widely used in rainfall-runoff simulation, flood forecasting, drought assessment, decision making, and water resources management (Corzo Perez et al., 2011; Tan et al., 2020; Wu et al., 2020; Gou et al., 2020,2021; Miao et al., 2022). Depending on the complexity of the model, hydrological models can be classified as conceptual (or lumped), semi-distributed, and distributed models (Beven, 1989; Jajarmizadeh et al., 2012; Khakbaz et al., 2012; Mai et al., 2022). Although current models simulate the hydrological processes well, they still suffer from multiple uncertainties, including input uncertainty, model structure and parameter uncertainty, and observation uncertainty (Nearing et al., 2016; Herrera et al., 2022). These uncertainties limit the accuracy of hydrological models (Honti et al., 2014; Sordo-Ward et al., 2016; Mai et al., 2022). Among them, input uncertainty is considered to be one of the largest sources of uncertainty. Precipitation, which is the driver of the water cycle, is the most important factor affecting streamflow simulation (Kobold and Sušelj, 2005).

Precipitation information is mainly derived from gauge observations, radar precipitation estimates and satellite precipitation retrievals (Sun et al., 2018). Gauge stations and radar are limited by the station network density and topography, especially in remote areas such as mountainous regions and high altitudes (Sun et al., 2018; Chen et al., 2020). Satellite precipitation estimation is the most promising hydrological model input with high spatial and temporal resolution at present (Jiang and Bauer-Gottwein, 2019; Dembélé et al., 2020). Several research institutions have developed various satellite precipitation estimation products with different data sources and algorithms, such as the Integrated Multi-satellitE Retrievals for Global Precipitation Measurement Mission (GPM IMERG) products jointly developed by the National Aeronautics and Space Administration (NASA) and Japan Aerospace Exploration Agency (JAXA) (Hou et al., 2013; Huffman et al., 2015), the Global Satellite Mapping of Precipitation (GSMaP) products developed by JAXA (Kubota et al., 2007, 2020), and the PDIR-Now product developed by the Center for Hydrometeorology and Remote Sensing (CHRS) at the University of California, Irvine (UCI) (Nguyen et al., 2020a, 2020b). However, there are still uncertainties in these products due to factors such as data sources and algorithms (Tian et al., 2009; Zhang et al., 2021a). And, the uncertainties are even amplified during the hydrological simulation (Cunha et al., 2012; Falck et al., 2015; Zhang et al., 2021b). This greatly limits the capability of satellite precipitation products for meteorological and downstream hydrological applications.

The current study addresses the uncertainty of satellite precipitation input in hydrological modeling in two ways, namely, pre-processing and post-processing (Wang et al., 2009; Ye et al., 2015; Li et al., 2017; Dong et al., 2020; Shen et al., 2021; Zhang et al., 2022a). Here~~, pre-processing and post-processing~~ we use the terminology of the hydrologic ensemble prediction experiment (HEPEX), where pre- and post-processing are distinguished before and after using the hydrological model (Schaake et al., 2007). That is, the precipitation input to the hydrological model and the streamflow output from the hydrological model are processed separately (Li et al., 2017). Hydrological pre-processing, also known as precipitation post-

https://doi.org/10.5194/hess-2022-377
Preprint. Discussion started: 21 November 2022
© Author(s) 2022. CC BY 4.0 License.

processing, is commonly used to obtain bias-corrected precipitation estimates by directly bias-correcting or fusing satellite precipitation estimates and gauge observations (Xu et al., 2020; Zhang et al., 2022a). The pre-processing mainly reduces the precipitation input uncertainty. The hydrological post-processing mainly uses the observed streamflow to correct the streamflow simulation or prediction (Ye et al., 2014; Tyralis et al., 2019). Hydrological post-processing not only reduces the effect of input uncertainty, or further reduces input uncertainty after hydrological pre-processing, but also reduces uncertainty caused by hydrological model structure and model parameters (Parrish et al., 2012; Kaune et al., 2020). Both hydrological pre-processing and post-processing can be used to generate predictions in a deterministic or probabilistic way. Probabilistic hydrological post-processing is the objective of this study.

In addition to the skewed distribution and heteroscedasticity, the streamflow time series have a strong autocorrelation (Herrera et al., 2022). According to this feature, there are two main types of methods used to perform hydrological post-processing. One is the autoregressive model based on residuals. Its main idea is to use the simulation residuals as forecast factors for the error update. Typical methods are error reduction models based on autoregression (Li et al., 2015, 2016; Zhang et al., 2018). Another way is to use the idea of model output statistics (MOS) (Wang et al., 2009; Bogner and Pappenberger, 2011). That is, the simulated streamflow is directly used as a forecasting factor to establish statistical relationships between simulations and observations. A representative approach of this type is the general linear model post-processor (GLMPP) (Zhao et al., 2011).

In recent years, machine learning (ML) and deep learning (DL) algorithms have become powerful tools for hydrological modeling (Sit et al., 2020; Zounemat-Kermani et al., 2021; Shen and Lawson, 2021; Fang et al., 2022). For example, Long-short memory (LSTM) models have been used to simulate streamflow in several gauged and ungauged basins in North America (Kratzert et al., 2018, 2019), the United Kingdom (Lees et al., 2021), and Europe (Nasreen et al., 2022). In addition to direct streamflow modeling, ML and DL algorithms can also be used as powerful hydrological post-processors for bias correction of streamflow simulation. For example, Frame et al. (2021) used LSTM to build a post-processor to correct the U.S. National Hydrologic Model and validated it on the CAMELS dataset containing 531 North American watersheds. The results showed that the LSTM post-processing significantly enhanced the output of the raw national hydrological model (Frame et al., 2021). Shen et al. (2022) used the random forest as a hydrological post-processor to enhance the simulation performance of the large-scale hydrological model PCR-GLOBAL model at three hydrological stations in the Rhine basin. Compared to deterministic forecasts, probabilistic forecasts can provide more uncertainty information to improve our risk management. In terms of probabilistic modeling, Tyralis et al. (2019) compared the usability of the statistical model (e.g., quantile regression) and the machine learning algorithm (e.g., quantile regression forests) as hydrological post-processors on the CAMELS dataset. And the results showed that the quantile regression forests model outperformed the quantile regression model. Zhu et al. (2020) investigated the applicability of LSTM for probabilistic hydrological forecasting with a Gaussian process model. Similarly, Althoff et al. (2021) quantified the uncertainty of LSTM for hydrological modeling using stochastic deactivation of neurons. Li et al. (2021, 2022) quantified the uncertainty of LSTM for hydrological modeling using variational inference from a Bayesian perspective. All these individual models can quantify the uncertainty information. More recently, Klotz et al. (2022)

https://doi.org/10.5194/hess-2022-377
Preprint. Discussion started: 21 November 2022
© Author(s) 2022. CC BY 4.0 License.

compared the application of dropout and three Gaussian mixture distribution models for uncertainty estimation in LSTM rainfall-runoff modeling. They found that the mixture density model outperformed the random dropout model, providing more reliable information on uncertainty. Both ML models and DL models have been successfully practiced in hydrological probabilistic post-processing. And some DL models have been compared and analyzed. However, there is no comparison between ML models and DL for hydrological probabilistic post-processing. DL models, while powerful, are often criticized for requiring large computational expenditures and time costs. ML models are more efficient but may perform poorly in comparison. However, we still do not know their differences in the field of hydrological probabilistic post-processing, such as the scope of application, model performance and computational efficiency.

Therefore, in this study, we attempt to fully compare the comprehensive performance of the two most widely used ML and DL models for streamflow probabilistic post-processing applications. The two models chosen are quantile regression forests (QRF) and probabilistic LSTM (PLSTM), respectively. We aim at sub-basin-scale daily streamflow probabilistic post-processing. In particular, a full model comparison is performed in a complex basin with 522 nested sub-basins in southwest China. Three sets of global satellite precipitation products are applied to generate uncorrected streamflow simulations. They are also used for single-feature and multi-feature input analysis. A variety of evaluation metrics are used to assess the proposed model performance, including probabilistic metrics for multi-point prediction and deterministic metrics for single-point prediction. The relationship between model performance and basin size is also analyzed according to the difference in the flow accumulation area of the sub-basin. This study can deepen our understanding of ML and DL models, and enable targeted model selection in practice.

2 Study area and Data

2.1 Study area

The Yalong River (Fig. 1a) is a major tributary of the Jinsha River, which belongs to the upper reaches of the Yangtze River. The Yalong River basin is located between the Qinghai-Tibet Plateau and the Sichuan Basin. The Yalong River basin has a long and narrow shape (96° 52’–102° 48’ E, 26° 32’–33° 58’ N), with snow-capped mountains scattered in the upper reaches, surrounded by high mountain valleys in the middle reaches, and flowing into the Jinsha River in the lower reaches. It spans seven dimensional zones with complex climate types. The total length of the basin is about 1,570 km, and the total area is about 130,000 km^2. The mean annual precipitation in the upstream and downstream is about 600 mm and 1,000 mm, respectively.

Following the watershed division method of Du et al. (2017), the whole Yalong River basin is divided to serval sub-basins with different catchment area. The key to sub-basin delineation is the minimum catchment area threshold, which is related to the total area of the basin, the model architecture complexity, the time scale and step size, the spatial resolution of the input data. Taking the above into consideration, the threshold is set to 100 km^2 in this study. As a result, the Yalong River

https://doi.org/10.5194/hess-2022-377
Preprint. Discussion started: 21 November 2022
© Author(s) 2022. CC BY 4.0 License.

basin is divided into 522 sub-basins (Fig. 1b). The location, elevation, area, flow accumulation area and flow direction of each sub-basin can be found in Table S1.

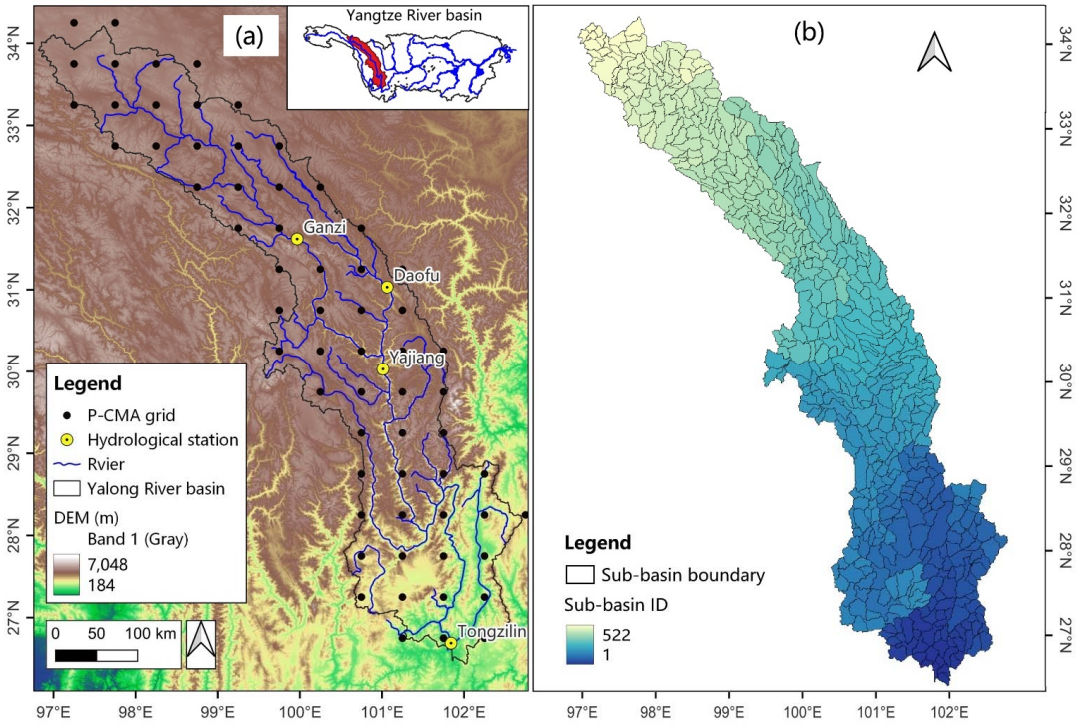

Figure 1. (a) Study area and (b) 522 sub-basins (**Zhang et al., 2022a**).

2.2 Data

2.2.1 Gauge precipitation observations

The 0.5-degree, daily precipitation observation data were obtained from the National Meteorological Information Center of the China Meteorological Administration (CMA-NMIC). The product was produced by interpolating gauge data from more than 2000 stations across China. This product has been verified to have high accuracy and has been widely applied to a variety of studies such as streamflow simulation, drought assessment, and water resources management (Gou et al., 2020, 2021; Zhang and Ye, 2021; Miao et al., 2022). In this study, the grid precipitation observations are used as a reference for the satellite-based precipitation products. Using the inverse distance weighting (IDW) method, they are interpolated to each sub-basin. And due to limited hydrological observatories, the streamflow of each sub-basin obtained from the calibrated hydrological model driven

https://doi.org/10.5194/hess-2022-377
Preprint. Discussion started: 21 November 2022
© Author(s) 2022. CC BY 4.0 License.

by this product is also used as a reference for the satellite precipitation-driven streamflow simulation. Errors caused by factors such as interpolation are ignored. The selected study period is from January 1, 2003 to December 31, 2018.

2.2.2 Global satellite precipitation estimates

Three sets of the latest quasi-global satellite precipitation estimate products are selected. The first one is the Precipitation Estimate from Remotely Sensed Information using Artificial Neural Networks-Dynamic Infrared Rain Rate near real-time (PDIR-Now, hereafter, PDIR), which solely relies on infrared data. Therefore it has a very high spatiotemporal resolution (0.04 degrees and 1 hour) and a very short delay time (1 hour), and it is a near real-time product without bias correction. The other two products are bias-adjusted products, IMERG Final Run version 6 (hereafter, IMERG-F) (Huffman et al., 2015, 2019) and Gauge-calibrated Global Satellite Mapping of Near real-time Precipitation product (GSMaP_Gauge_NRT_v6, hereafter, GSMaP) (Kubota et al., 2007, 2020), with a spatial resolution of 0.1 degrees. The selected study period is also from January 1, 2003 to December 31, 2018. All these products are aggregated to the daily scale and interpolated to each sub-basin using IDW method. The three precipitation products represent different research institutions and algorithms. Also, they have been proven to have relatively good accuracy in our previous study (Zhang et al., 2021b). It should be noted that these products are selected as examples only and any other precipitation product can be used as an alternative.

2.2.3 Other data

In addition to precipitation observations and satellite precipitation products, other meteorological data, basin attributes, and streamflow observations are needed for hydrological modeling. The meteorological data (including temperature, wind speed, etc.) were also obtained from the CMA-NMIC, and they are used to drive the hydrological model together with precipitation. The streamflow observations (January 1, 2006 to December 31, 2015) were collected from four gauged hydrological stations in the Yalong River basin from the upstream to the downstream, namely Ganzi (GZ), Daofu (DF), Yajiang (YJ), and Tongzilin (TZL). These data were obtained from the Hydrological Yearbook of the Bureau of Hydrology. The National Aeronautics and Space Administration Shuttle Radar Topographic Mission (NASA SRTM) digital elevation model (DEM) data with a spatial resolution of 90 m was obtained from the Geospatial Data Cloud of China. The 1 km soil data was clipped from the China Soil Database issued by the Tibetan Plateau Data Center of China. The 1km land use data was obtained from the Resource and Environment Science and Data Center provided by the Institute of Geographical Sciences and Resources, Chinese Academy of Sciences.

3 Methodology

3.1 Overview

The framework of this study is shown in Fig. 2. We adopt a two-stage streamflow post-processing approach. In the first stage, the hydrological model is calibrated and validated by hydrological station observations (Sect. 3.2.1). Then, we use the

https://doi.org/10.5194/hess-2022-377
Preprint. Discussion started: 21 November 2022
© Author(s) 2022. CC BY 4.0 License.

170 observed precipitation to drive the calibrated hydrological model to generate streamflow reference for each sub-basin (Sect. 3.2.2). And we use satellite precipitation to drive the model to generate uncorrected (raw) streamflow simulations (Sect. 3.2.3). In the second stage, we perform probabilistic post-processing of streamflow using the QRF model and the PLSTM model (Sect. 3.3). In the last subsection, we describe the scoring metrics used in this study (Sect. 3.4).

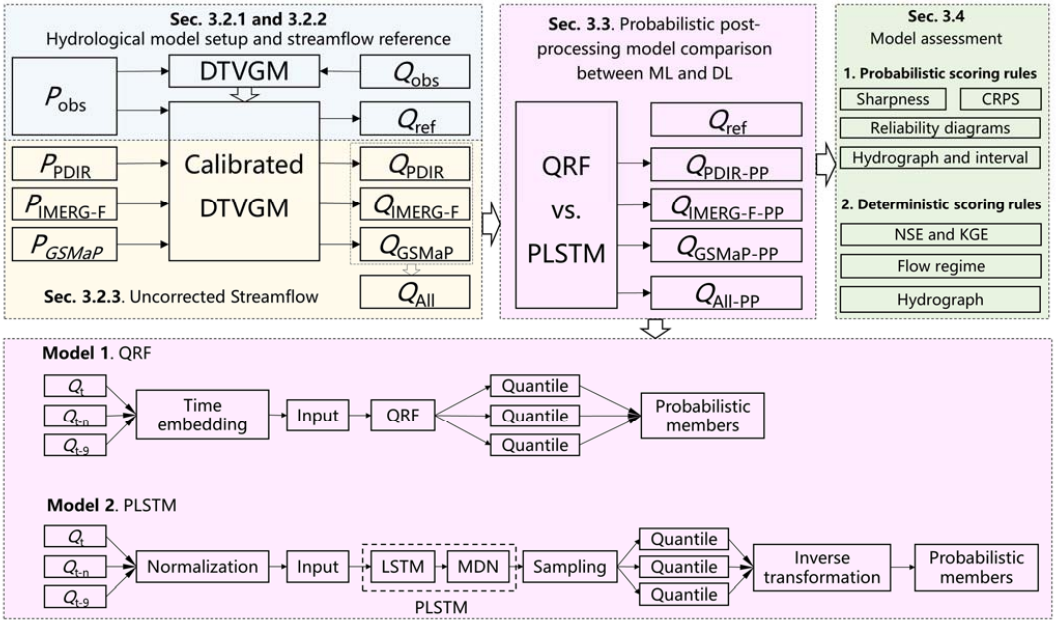

175 **Figure 2.** The framework of this study.

3.2 Streamflow reference and uncorrected streamflow simulations

3.2.1 Hydrological model setup, calibration and verification

The purpose of this study is to post-process the streamflow simulations for all sub-basin outlets, and therefore corresponding references are needed. Due to the limited streamflow observations, we use streamflow simulations from the 180 hydrological model driven by observed precipitation as a reference. To ensure that the results are reliable, we first use the collected streamflow observations from four hydrological stations to calibrate and validate the hydrological model.

We choose a hydrological model named distributed time-variant gain model (DTVGM) for rainfall-runoff simulation. The DTVGM is a distributed, process-based model that uses the rainfall-runoff nonlinear relationship (Xia, 1991; Xia et al., 2005). In each sub-basin, the runoff is calculated according to water balance. The kinematic wave equation is used for river

https://doi.org/10.5194/hess-2022-377
Preprint. Discussion started: 21 November 2022
© Author(s) 2022. CC BY 4.0 License.

routing (Ye et al., 2013). The snowmelt process in the high-altitude regions of the basin is simulated by the degree-day method (Bormann et al., 2014). A detailed description of the model can be found in (Xia et al., 2005; Ye et al., 2010).

Based on the length of the streamflow observation collected from hydrological stations (2006-2014, 9 years in total), we divide them into three periods: a one-year spin-up period (2006), a four-year calibration period (2007-2010), and a four-year validation period (2011-2014). We use Nash-Sutcliffe efficiency (NSE) as the objective and regionalize the parameters from upstream to downstream using manual tuning, while ensuring that the water balance coefficient converges to 1. The model calibration and validation are shown in Fig. S3. The NSE for the four gauged hydrological stations (GZ, DF, YJ, and TZL) are 0.89, 0.91, 0.93, 0.79, and 0.79, 0.86, 0.87, and 0.59 for the calibration and validation periods, respectively. The relatively poor performance of TZL during the validation period (2011-2014) is due to the downstream reservoir construction that changes the natural streamflow process. The used hydrological model does not include a reservoir regulation module, but we believe that the model is able to reproduce the natural runoff process well, so the model is reliable. More importantly, the observed precipitation-driven streamflow simulation is viewed as a reference. And in the post-processing stage, only the precipitation input is changed to compare the performance of the post-processing model to resolve the input uncertainty. Therefore, the errors caused by the model structure and model parameters are neglected.

3.2.2 Producing observed precipitation-driven streamflow simulation

After model calibration and validation, to ensure the number of data samples for data-driven post-processing methods, we use the observed precipitation from 2003 to 2018 to drive the hydrological model. A 16-year streamflow simulation reference data in 522 sub-basin outlets is finally obtained. Streamflow from different sub-basins can also reflect hydrological processes of diverse climate types and scales.

3.2.3 Producing satellite precipitation-driven uncorrected streamflow simulation

The uncorrected streamflow simulations are also needed before post-processing. Here we use three different satellite precipitation products (2003-2018) to drive the hydrological model separately to obtain three different streamflow simulations (PDIR, IMERG-F and GSMaP). In addition, the equal weight average of the three outputs can be seen as a multi-model (All) simulation. We do this for two considerations, first, the model performance of two different post-processing models can be adequately compared in three different contexts. Secondly, the multi-model inputs can be used to compare the effects of model averaging and multi-dimensional features on the post-processing models.

3.3 Hydrological post-processing procedure

In this section, we present the two probabilistic post-processing models compared in this study. Flowcharts of the two post-processing models can also be found in the bottom panel of Fig. 2. The principles of the two models are briefly described in Sect. 3.3.1 and Sect. 3.3.2. Model setup, including feature selection, hyperparameters and experiments are in Sect. 3.3.3. The probabilistic members are generated by the post-processing model in Sect. 3.3.4.

https://doi.org/10.5194/hess-2022-377
Preprint. Discussion started: 21 November 2022
© Author(s) 2022. CC BY 4.0 License.

3.3.1 QRF

Random forests (RF) is an ensemble machine learning (ML) algorithm based on decision trees (Li et al., 1984; Breiman, 2001). Three steps are required to implement the RF model. First, we start by splitting the total samples and sampling K subsamples for K individual decision trees. Then each decision tree makes its own prediction. Finally, multiple decision trees are averaged or voted to get the final prediction. Compared to decision trees, random forests provide two additional randomness: (1) random sampling of samples, and (2) parallel integration of multiple decision trees. Therefore, the random forests can correct the inductive preferences induced by individual decision trees from falling into local optima, thus effectively preventing overfitting.

However, the prediction made using RF regression is the conditional mean of the target variable. This means that the RF model will ignore the entire conditional probability distribution. By introducing quantiles, the RF model produces a variant of quantile regression forests (QRF) (Meinshausen and Ridgeway, 2006). The QRF model considers the distribution of the entire data by selecting different quantiles, and therefore is able to generate probabilistic members. A more detailed description of RF and QRF models can be found in Zhang et al. (2022a). QRF model has been widely used in several studies (Taillardat et al., 2016; Evin et al., 2021; Kasraei et al., 2021; Tyralis et al., 2019; Tyralis and Papacharalampous, 2021).

3.3.2 PLSTM

Long short-term memory (LSTM) network is one of the most famous recurrent neural networks (RNNs), and it is a representative of sequential deep learning (DL) algorithms (Staudemeyer and Morris, 2019). RNN models are designed to effectively utilize temporal information and have a wide range of applications in speech recognition and speech translation (Hori et al., 2018). However, the original RNN model is prone to gradient vanishing as the time series grows, leading to model failure to converge. LSTM effectively solves the gradient problem by introducing gate functions. The LSTM model has been widely used in various fields such as rainfall-runoff simulation and soil moisture simulation (Fang et al., 2017, 2022; Kratzert et al., 2018, 2019; Fang and Shen, 2020). The formulas of LSTM can be found in the previous studies (Fang et al., 2017; Kratzert et al., 2018; Staudemeyer and Morris, 2019).

Similar to the RF model, the LSTM model can only make deterministic predictions and cannot provide probabilistic information. There are currently several methods in the literature to quantify the uncertainty of LSTM and thus give probabilistic predictions. In a recent study, Klotz et al. (2022) compared four different methods, including three mixture density networks (MDNs) and one Monte Carlo dropout (MCD) method. A mixture density is a probability density function created by combining multiple densities. In their studies, three forms of MDNs with different levels of complexity were adopted, namely, Gaussian mixture models (GMMs), Countable mixture of asymmetric Laplacians (CMAL) and Uncountable mixtures of asymmetric Laplacians (UMAL). MCD randomly changes the number of neurons through multiple experiments to obtain probabilistic outputs. The complexity of CMAL is between that of GMM and UMAL, and it achieved the best performance in

https://doi.org/10.5194/hess-2022-377
Preprint. Discussion started: 21 November 2022
© Author(s) 2022. CC BY 4.0 License.

the study of Klotze et al. (2022). Therefore, we choose CMAL as a representative of PLSTM in this study. A detailed description of CMAL can be found in Klotz et al. (2022) and will not be repeated in this study.

3.3.3 Model setup and experimental design

Both post-processing models require input features. Here, to maintain the low complexity of the model, we select only the uncorrected streamflow as input features. Considering the autocorrelation of the streamflow (see Fig. S2), for the post-processing on day t (Q_t), we select the simulated streamflow for the first 9 days (Q_{t-9}^{sim}, Q_{t-8}^{sim},…, Q_{t-1}^{sim}) and the simulated streamflow of that day (Q_t^{sim}) as the inputs. In the RF model, the input features are fed by temporal embedding. And in the LSTM model, the seq-length is set to 9. For both models, we select the streamflow reference on day t (Q_t^{ref}) as the target. In addition, since we used three different satellite precipitation products, the experiments are divided into a single-model experiment and a multi-model experiment (All). The information of each experiment is summarized in Table 1.

Table 1. Experimental design.

Streamflow simulation	Model	Input feature	~~Dimension~~	Target
PDIR	QRF	Q_{t-9}^{sim}, Q_{t-8}^{sim},…, Q_t^{sim}	10	Q_t^{ref}
	PLSTM		1	
IMERG-F	QRF		10	
	PLSTM		1	
GSMaP	QRF		10	
	PLSTM		1	
All (PDIR, IMERG-F, GSMaP)	QRF		30	
	PLSTM		3	

The training period is from 1 January 2003 to 31 December 2010. The validation period is from 1 January 2011 to 31 December 2014. And the test period is from 1 January 2015 to 31 December 2018.

We implement the QRF model using *pyquantrf* package (Jnelson18, 2022). We tuned three sensitive hyperparameters in the QRF model through grid search, finally set the number of trees (K) ~~is~~ 70, the number of non-leaf node splitting features ~~is~~ 10, and the number of samples used for leaf node predictions (N_{leaf}) ~~is~~ 10. The other hyperparameters are set to default values.

We implement the PLSTM model using *NeuralHydrology* package (Kratzert et al., 2022a). We follow the model architecture of Klotz et al. (2022), which contains an LSTM layer and a CMAL layer. Unlike the QRF model, the input data of the PLSTM model needs to be normalized. Here, by several comparisons, we use the normal quantile transform (Fig. S3). The model hyperparameters include the number of neurons in the LSTM layer (N_{LSTM}), the number of components of the mixture density function (N_{MDN}), the dropout rate, the learning rate, the epoch, and the batch size. For N_{MDN}, we set it to 3,

https://doi.org/10.5194/hess-2022-377
Preprint. Discussion started: 21 November 2022
© Author(s) 2022. CC BY 4.0 License.

which is the same as Klotz et al. (2022). We fine-tuned the other hyperparameters. The final learning rate is 0.0001, the dropout is 0.4, the epoch is 100, the batch size is 256, and the N_{LSTM} is 256.

Our computing platform is a workstation configured with an Intel(R) Xeon(R) Gold 6226R CPU @ 2.9GHz and an RTX3090 GPU with 24G video memory. It is important to note that we model each sub-basin separately. This is because the PLSTM model generates probabilistic members with random sampling exceeding the GPU's video memory (see Sect. 3.3.4 and Sect. 5.3). For consistency, the QRF model is also modelled locally. It takes approximately 12 hours to complete all PLSTM experiments. It takes about 6 hours to complete all QRF experiments.

3.3.4 Producing probabilistic members

For the QRF model, we equally sample 100 quantiles (0.005 to 0.995) for each basin and time step and bring them directly into the model to obtain the final probabilistic (100) members. For the PLSTM model, we first sample from the mixture distribution to get 10,000 sample points for each basin and time step. We then take the same 100 quantiles (0.005 to 0.995) from these sample points, remap them to original streamflow space using inverse quantile normal transformation, and finally produce the probabilistic (100) members.

3.4 Performance measures

We evaluate the two post-processing models from both probabilistic and deterministic perspectives. The scoring metrics are presented in Sect. 3.4.1 and Sect. 3.4.2, respectively.

3.4.1 Probabilistic (multi-point) metrics

The evaluation of probabilistic post-processing uses metrics that describe the accuracy, reliability, and sharpness.

1) Continuous rank probability score (CRPS)

The continuous rank probability score (CRPS) is widely used in probabilistic evaluations (Bröcker, 2012). For given probabilistic members, the CRPS calculates the difference between the cumulative distribution function (CDF) of the probabilistic members and the observation. It can be used for a comprehensive assessment of the accuracy, reliability and sharpness of probabilistic forecasts (Bröcker, 2012). The CRPS is also the basic metric for evaluating the goodness of probabilistic outputs in this study. For different thresholds focused on the evaluation of extreme events, we also chose threshold weighted CRPS (hereafter twCRPS, Gneiting and Ranjan, 2011; Zhao et al., 2022). The two metrics can be expressed as:

$$CRPS = \int_{-\infty}^{\infty} \left(F(Q_t) - O(Q_t)\right)^2 dP_t \tag{1}$$

$$twCRPS = \int_{-\infty}^{\infty} \left(F(Q_t) - O(Q_t)\right)^2 \omega(Q) dQ_t \tag{2}$$

https://doi.org/10.5194/hess-2022-377
Preprint. Discussion started: 21 November 2022
© Author(s) 2022. CC BY 4.0 License.

where $\omega(Q)$ is a threshold weighted function and is calculated based on the threshold q (80%, 90% and 95% in this study). When $Q \geq q$ (or $Q < q$), $\omega(Q)$ equals 1 (or 0) if. P_t is a streamflow reference threshold; $O(Q_t)$ is the CDF obtained from the probabilistic outputs for day t; $F(Q_t)$ is the Heaviside function, and it can be expressed as:

$$O(Q_t) = \begin{cases} 1, & O_i > Q_t \\ 0, & O_i \leq Q_t \end{cases} \tag{3}$$

where O_i is i^{th} probabilistic members, and Q_t is the corresponding reference. The better performing model has both metrics (CRPS and twCRPS) closer to 0.

We also used the CRPS score (CRPSS) to define the relative differences between the two post-processing models. For example, for QRF and PLSTM, the CRPSS can be calculated using the following Eq. (4):

$$CRPSS_{QRF/PLSTM} = \left(1 - \frac{CRPS_{QRF}}{CRPS_{PLSTM}}\right) \times 100\% \tag{4}$$

The CRPSS is greater than 0, indicating that the QRF model is better than the PLSTM model; conversely, the PLSTM model is better than the QRF model.

2) Reliability diagram

The reliability diagram is used to assess the conformity between the predicted probability and its observed frequency (Hartmann et al., 2002). A perfectly reliable prediction will match the diagonal line (1:1). A forecast point above (or below) the diagonal line indicates an underestimation (or overestimation). Here again, three thresholds (80%, 90%, and 95%) are chosen to better evaluate the reliability of heavy flood events (Yang et al., 2021).

3) Sharpness

Predict intervals are often used to describe the sharpness of probabilistic forecasts (Gneiting et al., 2007). The 50% and 90% quantile intervals were chosen in this study. In addition, we calculated the coverage of the predict intervals over the observations. And we also selected serval metrics used in previous study (Klotz et al., 2022), including Mean absolute deviation (MAD), Standard deviation (STD) and Variance (VAR).

3.4.2 Deterministic (single-point) metrics

The widely used and standard scoring metrics (e.g., Nash-Sutcliffe efficiency, NSE and Kling-Gupta efficiency, KGE) are applied for assessing deterministic hydrological modeling (Nash and Sutcliffe, 1970; Kling et al., 2012). Two components (Pearson correlation coefficient, PCC and relative bias, RB) of NSE are also calculated to describe the consistency and systematic bias of the difference between simulation and observations, respectively.

In addition, due to the seasonality, four metrics are selected to describe the different flow regimes, including the peak flow bias (FHV, Eq. (A3) in Yilmaz et al., 2008) (Yilmaz et al., 2008), the low-flow bias (FLV, Eq. (A4) in Yilmaz et al., 2008), the flow duration curve bias (FMS, Eq. (A2) in Yilmaz et al., 2008), and mean peak time lag bias (in days) (PT, Appendix D in Kratzert et al., 2021).

https://doi.org/10.5194/hess-2022-377
Preprint. Discussion started: 21 November 2022
© Author(s) 2022. CC BY 4.0 License.

4 Results

4.1 Uncorrected streamflow simulations

Figure 3 shows the spatial performance (NSE) of the streamflow simulations driven by three different satellite precipitation products and multi-model outputs equal-weighting averaging (All). Among the three satellite precipitation products, IMERG-F achieves the best model performance, followed by PDIR and GSMaP. PDIR performs poorly in the upstream and outlet regions of the basin. GSMaP differs significantly from streamflow reference in almost all sub-basins. Direct simple model averaging (SMA), which introduces biased information of PDIR and GSMaP, does little to improve model performance.

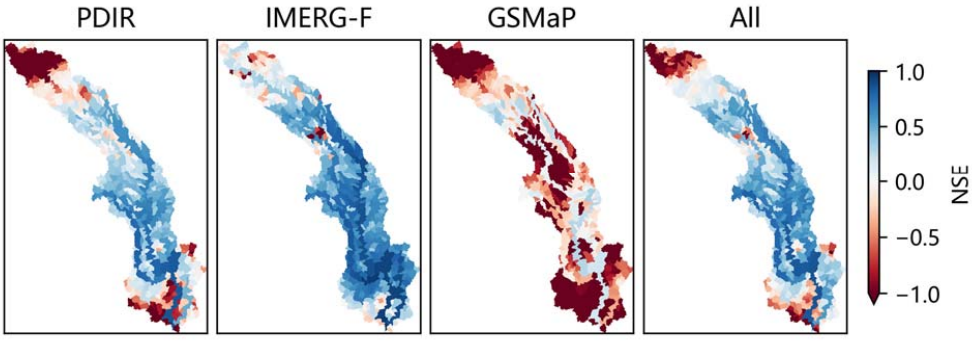

Figure 3. The performance (Nash-Sutcliffe efficiency, NSE) of uncorrected (raw) streamflow simulation. The closer the NSE is to 1, the better the model performs. PDIR is a near real-time product; IMERG-F and GSMAP are bias-adjusted products.

4.2 Probabilistic (multi-point) assessment

The flow magnitudes in different sub-basins vary widely. Therefore, when we present the results for all sub-basins, we normalize the results for each sub-basin separately according to the probabilistic membership of all experiments. By doing so, the probabilistic members of all sub-basins are unified to the range of 0 to 1.

4.2.1 CRPS and twCRPS overall performance

In general, the performance (CRPS and twCRPS) of the QRF and PLSTM models is similar for all threshold conditions (Fig. 4). However, it is worth noting that the QRF model has more outliers in contrast to the PLSTM model. For different precipitation-driven streamflow inputs, the post-processing performance of the bias-corrected product (e.g., IMERG-F) is better than that of the near-real-time product (e.g., PDIR). In the category of bias-corrected products, IMERG-F gives better results than GSMaP. This indicates the value of bias correction of precipitation products as a pre-processing tool for hydrological simulations. At the same time, high-quality precipitation forcing is helpful for both streamflow simulation as well as probabilistic post-processing. The multi-model results (All) are similar to the best-performing single-model results

https://doi.org/10.5194/hess-2022-377
Preprint. Discussion started: 21 November 2022
© Author(s) 2022. CC BY 4.0 License.

(IMERG-F). However, they are slightly worse than IMERG-F above the 90% threshold This suggests that the input of multiple models, especially when the single model performs poorly, may have a negative effect on the post-processing.

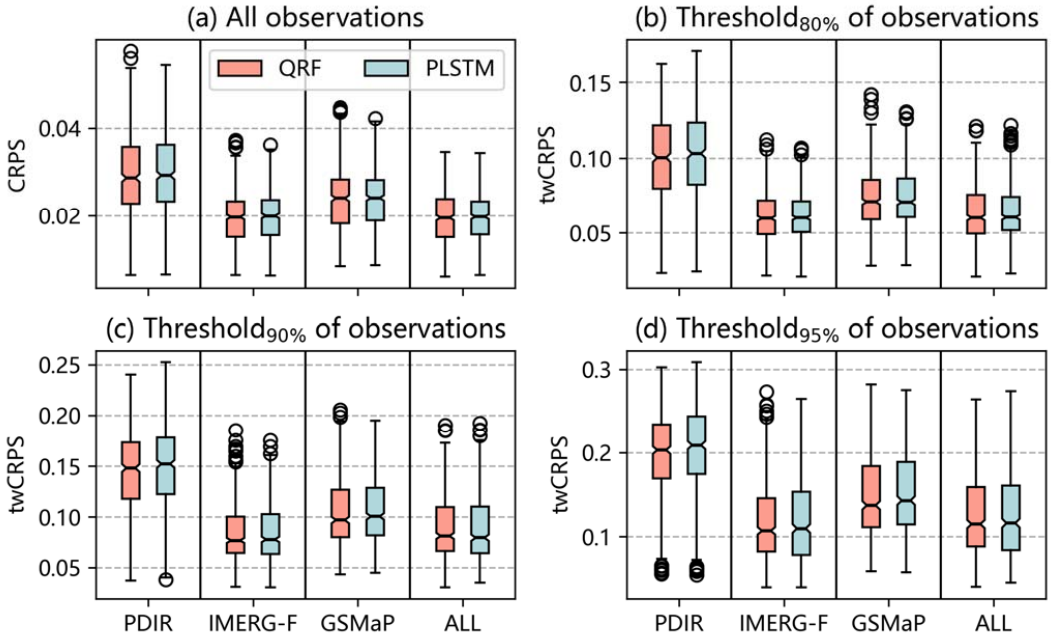

Figure 4. The continuous rank probability score (CRPS) and twCRPS overall performance. The better performing model has both metrics closer to 0. PDIR is a near real-time product; IMERG-F and GSMAP are bias-adjusted products.

4.2.2 CRPS spatial distribution

In addition to their overall performance (Fig. 4), the QRF and PLSTM models exhibit similar spatial distributions (Fig. 5). Compared to PDIR and GSMaP, IMERG-F and multi-model results achieve relatively good performance in most of the 522 sub-basins. PDIR performs poorly in the middle and lower reaches of the basin. The third row of the figure (Fig. 5) shows that the difference between QRF and PLSTM is mostly within 10%. However, the introduction of multiple models increases the gap between them.

https://doi.org/10.5194/hess-2022-377
Preprint. Discussion started: 21 November 2022
© Author(s) 2022. CC BY 4.0 License.

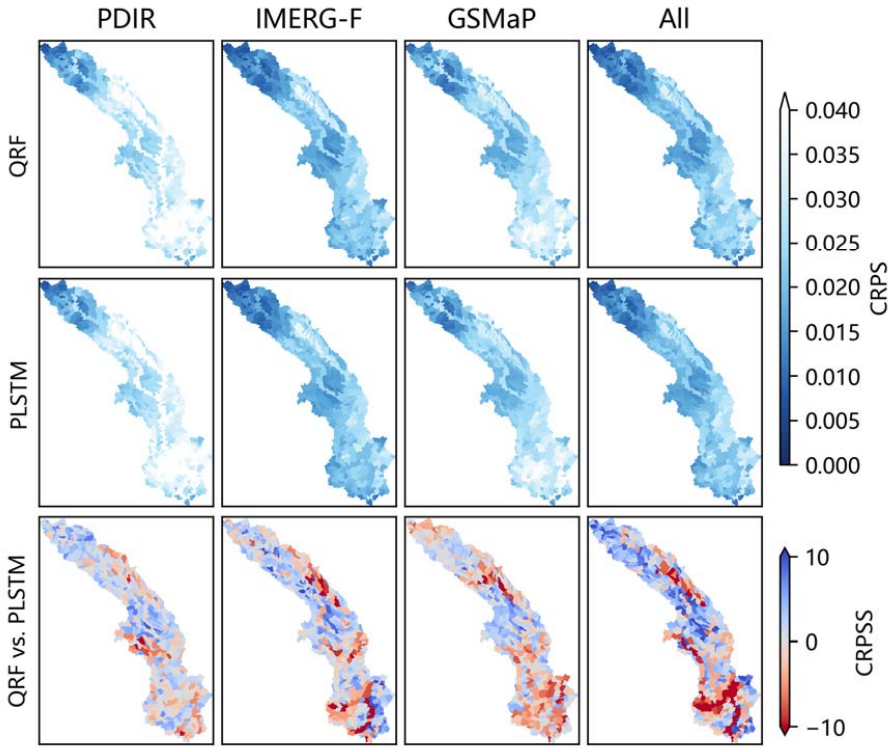

Figure 5. The continuous rank probability score (CRPS) and CRPS score (CRPSS) spatial distributions. The closer the CRPS is to 0, the better the model performs. The CRPSS is greater than 0, indicating that the QRF model performs better than PLSTM; conversely, the PLSTM model performs better than QRF. PDIR is a near real-time product; IMERG-F and GSMAP are bias-adjusted products.

4.2.3 The relationship between model performance and flow accumulation area

The spatial variation of CRPS and CRPSS seems to be irregularly and scattered distributed. To further investigate the model difference, we analyze the relationship between CRPS, CRPSS and the flow accumulation area (FAA) of the sub-basin. The results are presented in Fig. 6. We can observe the interesting phenomenon that there is a scale effect in the performance of different models. In the sub-basins with flow accumulation area (FAA) less than 20,000 km^2, the performance of QRF and PLSTM is disorderly scattered, with high and low CRPS values (Fig. 6a). But, as the flow accumulation area (FAA) of the sub-basin increases, the value of CRPS stabilizes when the FAA is greater than 20,000 km^2.

https://doi.org/10.5194/hess-2022-377
Preprint. Discussion started: 21 November 2022
© Author(s) 2022. CC BY 4.0 License.

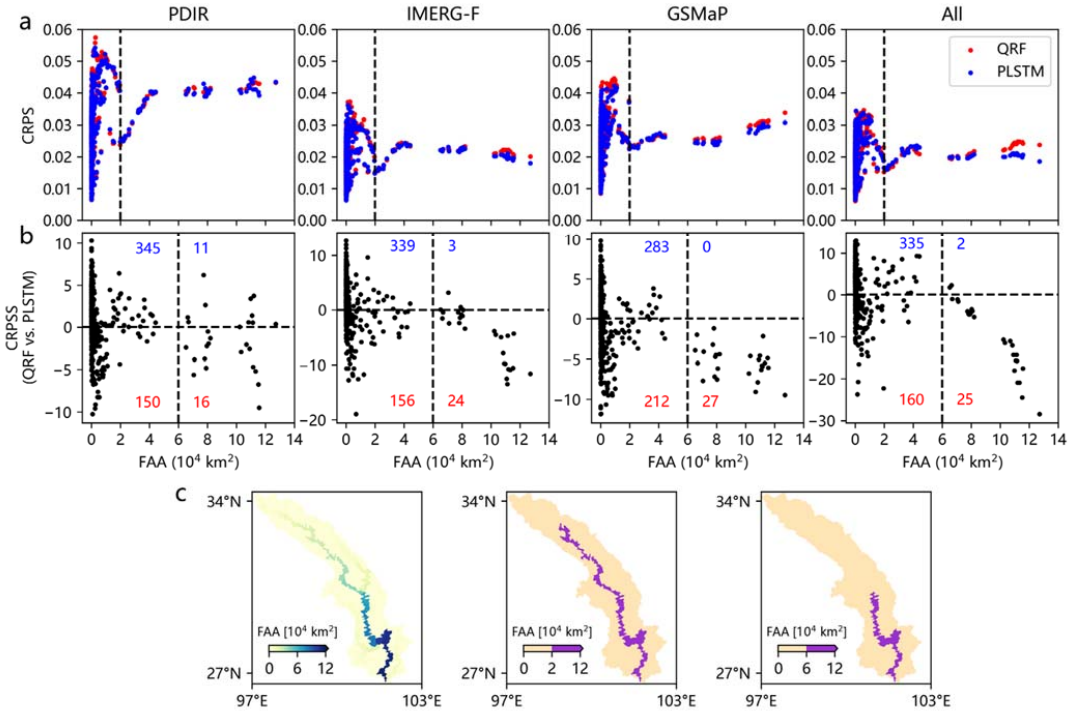

Figure 6. The relationships between (a) continuous rank probability score (CRPS), (b) CRPS score (CRPSS) and (c) flow accumulation area (FAA). The closer the CRPS is to 0, the better the model performs. The CRPSS is greater than 0, indicating that the QRF model is better than the PLSTM model; conversely, the PLSTM model is better than the QRF model. PDIR is a near real-time product; IMERG-F and GSMAP are bias-adjusted products.

In addition, there is also a very clear dividing line between the performance of the QRF and LSTM models (Fig. 6b). If we divide this scatter plot into four quadrants, quadrants 1,2 represent the QRF model better than the PLSTM model (blue number), and quadrants 3,4 represent the QRF model worse than the PLSTM model (red number). When the flow accumulation area (FAA) of the sub-basin is less than 60,000 km^2, the QRF model is a little more dominant than the PLSTM model. But in sub-basins with flow accumulation area (FAA) greater than 60,000 km^2, the PLSTM model shows overwhelming performance. This feature is most pronounced in the GSMaP-driven streamflow post-processing, followed by multi-model (All), IMERG-F and PDIR.

https://doi.org/10.5194/hess-2022-377
Preprint. Discussion started: 21 November 2022
© Author(s) 2022. CC BY 4.0 License.

4.2.4 Reliability diagrams

To distinguish the difference in model performance between the PLSTM model and the QRF model as the flow accumulation area (FAA) changes, we split the calculation of the reliability diagrams into two parts, one for the FAA less than 60,000 km^2 (Fig. 7) and one for the FAA greater than 60,000 km^2 (Fig. 8).

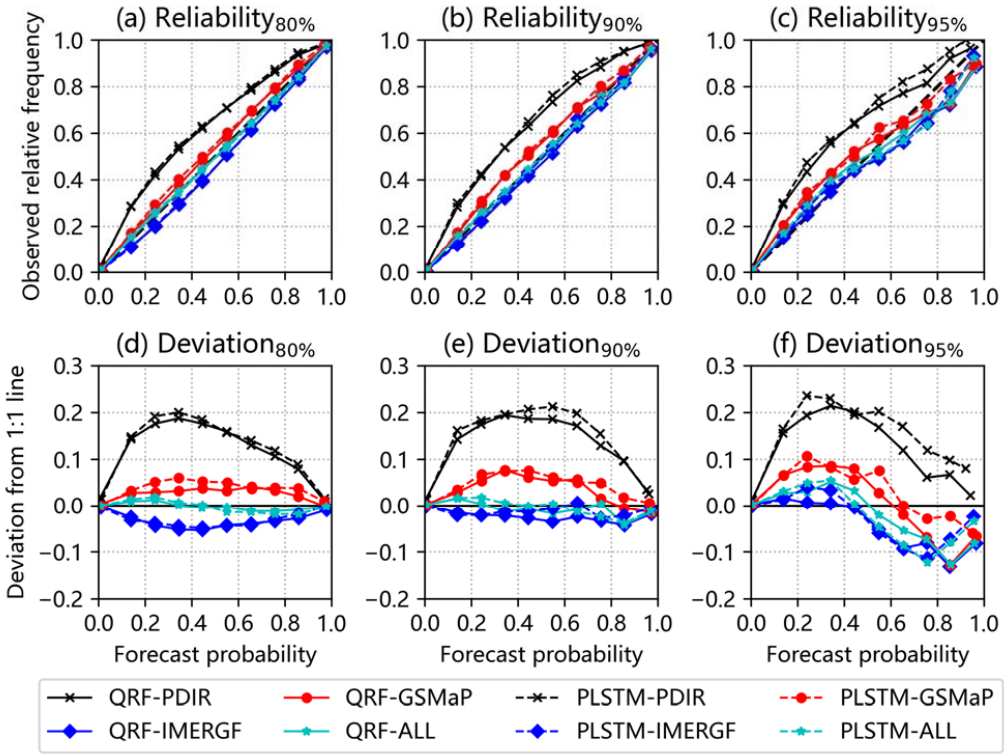

Figure 7. Reliability diagrams (a-c) and deviation (d-f) from 1:1 line between different models for sub-basins with flow accumulation area (FAA) less than 60,000 km^2. PDIR is a near real-time product; IMERG-F and GSMAP are bias-adjusted products.

Figure 7 shows the reliability plots of different models for sub-basins with flow accumulation area (FAA) less than 60,000 km^2 and their deviations from the diagonal (1:1 line). Also, we selected 80%, 90% and 95% quartiles of the observation as the threshold conditions, respectively. And the reliability plots are calculated by combing all streamflow simulations from 495 sub-basins with FAA less than 60,000 km^2. In general, the two post-processing methods perform close to each other. The QRF model (solid line) is slightly better than PLSTM (dashed line), with a relatively smaller deviation from the diagonal (1:1 line). All experiments have high reliability except for the one with PDIR-driven streamflow simulation as input. As the threshold

https://doi.org/10.5194/hess-2022-377
Preprint. Discussion started: 21 November 2022
© Author(s) 2022. CC BY 4.0 License.

increases, the deviation of all experiments from the diagonal increases and the reliability level decreases. Among the different experiments, IMERG-F is the best. Multi-model (All) is close to IMERG-F but slightly worse. But they both show some degree of underestimation. The GSMaP is the second best and the PDIR the worst. The GSMaP and PDIR show some degree of overestimation. These results can also explain the differences in CRPS of different models.

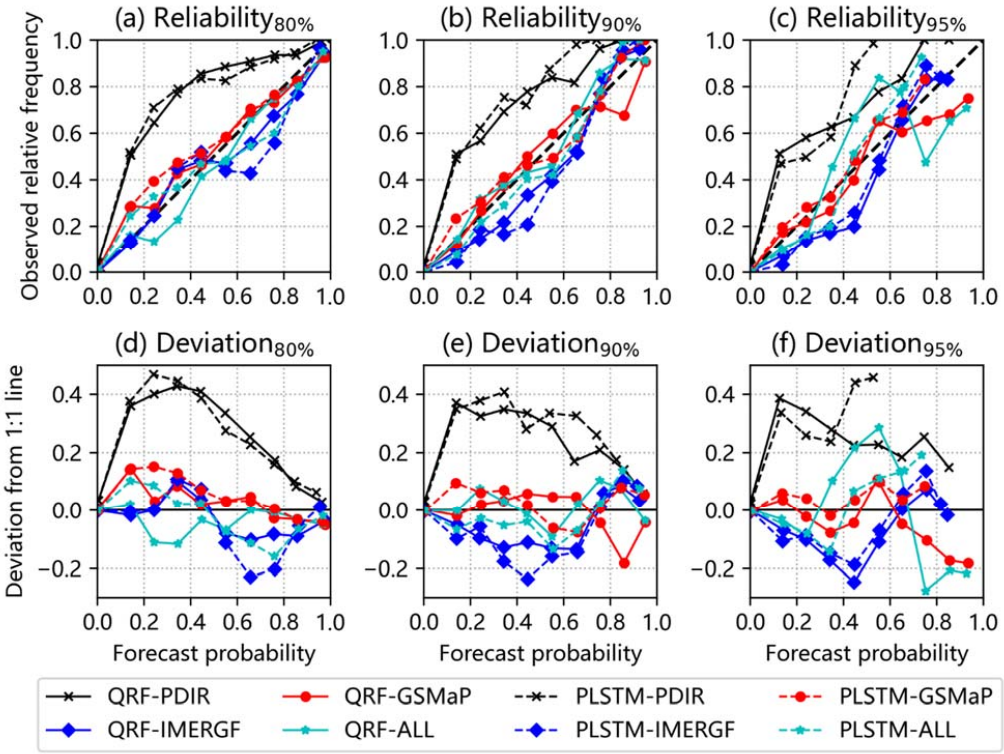

Figure 8. Same with Fig. 7, but for sub-basins with flow accumulation area (FAA) larger than 60,000 km^2. PDIR is a near real-time product; IMERG-F and GSMAP are bias-adjusted products.

Figure 8 shows the reliability plots of different models for sub-basins with flow accumulation area (FAA) larger than 60,000 km^2 and their deviations from the diagonal (1:1 line). Also, we selected 80%, 90% and 95% quartiles of the observation as the threshold conditions, respectively. And the reliability plots are calculated by combing all streamflow simulations from 27 sub-basins with FAA greater than 60,000 km^2. In general, the two post-processing methods show distinguishable differences in this case. The PLSTM (dashed line) is slightly better than QRF (solid line), possessing more points distributed around the diagonal (1:1 line). However, both models exhibit greater uncertainty in this case relative to the FAA of sub-basins smaller than 60,000 km^2 (Fig. 7). As the threshold increases, the deviation of all experiments from the diagonal increases, the curve

https://doi.org/10.5194/hess-2022-377
Preprint. Discussion started: 21 November 2022
© Author(s) 2022. CC BY 4.0 License.

becomes more oscillatory, and the reliability level is greatly reduced, especially in extreme cases (Fig. 8f, 95% quantile threshold). Similar to Fig. 7, among the different experiments, IMERG-F is still the best and Multi-model (All) is close to IMERG-F, but slightly worse. They all show more underestimation. The GSMaP is the second best and PDIR the worst. Except a few points, they show more overestimation.

4.2.5 Sharpness

In order to compare the model performance of PLSTM and QRF more comprehensively, this section further calculates the sharpness metrics for different experiments. The selected sharpness metrics include: mean absolute deviation (MAD), standard deviation (STD), variance (VAR), distance from 25% to 75% quantile (DIS25-75), distance from 5% to 95% quantile (DIS5-95), coverage of observations by 25% to 75% quantile (CO25-75), and coverage of observations by 5% to 95% quantile (CO5-95). In addition, to remove the effect of different flow regimes, all data are divided into a high flow season (May to October) and a low flow season (November to April). Sharpness metrics are calculated separately for each sub-basin. The mean results for all 522 sub-basins are presented in Table 2.

Table 2. Sharpness metrics (Mean absolute deviation, MAD; Standard deviation, STD; Variance, VAR; Distance between the 0.25 and 0.75 quantiles, $DIS_{25\text{-}75}$; Distance between the 0.05 and 0.95 quantiles, $DIS_{5\text{-}95}$; Coverage of observations between the 0.25 and 0.75 quantiles, $CO_{25\text{-}75}$; Coverage of observations between the 0.05 and 0.95 quantiles, $CO_{5\text{-}95}$) for different models. The bold numbers indicate better performance in each group.

Flow seasons	Metric	PDIR		IEMRG-F		GSMaP		All	
		QRF	PLSTM	QRF	PLSTM	QRF	PLSTM	QRF	PLSTM
High-flow (May–Oct.)	MAD	**0.046**	0.048	**0.047**	0.052	**0.050**	0.054	**0.045**	0.047
	STD	**0.109**	0.112	**0.133**	0.139	**0.129**	0.133	**0.129**	0.134
	VAR	**0.013**	0.014	**0.020**	0.021	**0.018**	0.019	**0.018**	0.020
	$DIS_{25\text{-}75}$	0.0714	**0.0703**	**0.0753**	0.0757	**0.0781**	0.0785	0.0710	**0.0687**
	$DIS_{5\text{-}95}$	**0.184**	0.194	**0.192**	0.215	**0.206**	0.223	**0.184**	0.195
	$CO_{25\text{-}75}$ (%)	**51.5**	50.1	**76.9**	76.0	**64.2**	62.8	**73.3**	71.4
	$CO_{5\text{-}95}$ (%)	100	100	100	100	100	100	100	100
Low-flow (Nov.–Apr.)	MAD	**0.0085**	0.0100	**0.0073**	0.0094	**0.0088**	0.0104	**0.0064**	0.0069
	STD	**0.0264**	0.0284	**0.0280**	0.0301	**0.0305**	0.0323	**0.0258**	0.0262
	VAR	**8.32**	9.48	**9.10**	10.47	**10.40**	11.52	**7.71**	7.86
	$DIS_{25\text{-}75}$	**0.0121**	0.0124	**0.0099**	0.0112	**0.0121**	0.0122	0.0086	**0.0086**
	$DIS_{5\text{-}95}$	**0.033**	0.039	**0.029**	0.037	**0.036**	0.042	**0.026**	0.027
	$CO_{25\text{-}75}$ (%)	72.2	**75.1**	88.8	**90.2**	69.1	**73.9**	**79.6**	79.2
	$CO_{5\text{-}95}$ (%)	100	100	100	100	100	100	100	100

As can be found in Table 2, the QRF model obtained narrower quantile intervals for both high and low flows in the average of all 522 sub-basins, representing a higher sharpness of the QRF model. It is noteworthy that the QRF model performs both a narrower quantile interval and coverage of observations in the high-flow season. For the coverage of observations from the 25th to the 75th percentile (CO25-75), the QRF model is on average 1.5% higher than the PLSTM. However, the wider

https://doi.org/10.5194/hess-2022-377
Preprint. Discussion started: 21 November 2022
© Author(s) 2022. CC BY 4.0 License.

quantile interval of PLSTM yields higher coverage of observations in the low-flow season. For the 25% to 75% quantile coverage of observations (CO25-75), the PLSTM is on average 2% higher than the QRF model. Surprisingly, the 5%-95% quantile interval obtained by the two post-processing methods contains 100% of the observations for both high and low flows in the average of all 522 sub-basins.

4.2.6 Hydrograph and predict interval of two typical sub-basins

Table 2 shows the average sharpness performance of all sub-basins. In this section, two typical sub-basins are selected as individual examples to explain in detail the performance differences between PLSTM and QRF models. Sub-basin No.10 and No.250 are from quadrant 4 and quadrant 2 of Fig. 6, respectively. The overall performance (CRPS) of the PLSTM model in sub-basin No.10 is better than that of the QRF, but it is worse than the QRF in sub-basin No.250.

Figure 9 shows the hydrographs and two different quantile intervals for different experiments. Corresponding to Fig. 9, Table 3 shows a statistical summary of the indicators of quantile intervals and their coverage of observations. Similarly, in both cases, the QRF and PLSTM models exhibit smaller prediction uncertainty and present narrower quantile intervals in the low-flow season (Nov. to Apr.). While in the high-flow season (May to Oct.), the prediction uncertainty is larger. Moreover, the narrower uncertainty intervals in the low-flow season yielded higher coverage of observations. The difference is that in sub-basin No.10, the PLSTM model obtains a higher coverage of observations at the expense of some sharpness. It strikes a balance between the prediction interval and the coverage of observations, which results in a higher CRPS. In contrast, the QRF model suffers from systematic errors despite its narrower prediction interval. For example, the systematic underestimation of QRF-IMERG-F in the high-flow season results in lower CRPS relative to PLSTM. For sub-basin No.250 with a smaller flow accumulation area (FAA), its concentration time is short, the flow variation is more fluctuating and complicated, and the observation points are more scattered. Little precipitation events may also cause high pulse flow, which is also the main feature of flash flood disasters. Interestingly, in this case, the QRF wraps more observations with a narrower quantile interval, which results in higher CRPS for them.

Table 3. Sharpness metrics (Distance between the 0.25 and 0.75 quantiles, $DIS_{25\text{-}75}$; Distance between the 0.05 and 0.95 quantiles, $DIS_{5\text{-}95}$; Coverage of observations between the 0.25 and 0.75 quantiles, $CO_{25\text{-}75}$; Coverage of observations between the 0.05 and 0.95 quantiles, $CO_{5\text{-}95}$) for different models in two typical sub-basins. The bold numbers indicate better performance in each group.

ID	Input	Model	High flow seasons (May–Oct.)				Low flow seasons (Nov.–Apr.)			
			$DIS_{25\text{-}75}$ (m^3/s)	$DIS_{5\text{-}95}$ (m^3/s)	$CO_{25\text{-}75}$ (%)	$CO_{5\text{-}95}$ (%)	$DIS_{25\text{-}75}$ (m^3/s)	$DIS_{5\text{-}95}$ (m^3/s)	$CO_{25\text{-}75}$ (%)	$CO_{5\text{-}95}$ (%)
10	PDIR	QRF	**596.8**	**1491.5**	28.8	60.9	**113.4**	**232.6**	40.0	76.1
		PLSTM	676.4	1765.9	**33.0**	**68.6**	124.7	345.1	**56.4**	**97.0**
	IEMRG-F	QRF	**634.5**	**1576.2**	40.5	82.7	**72.6**	**186.1**	41.9	78.5
		PLSTM	670.7	1879.5	**53.8**	**92.5**	139.0	327.5	**57.8**	**94.5**
	GSMaP	QRF	**825.5**	**1755.8**	**39.3**	71.3	**125.1**	**275.8**	41.8	68.0
		PLSTM	762.5	1921.5	33.4	**81.9**	130.0	398.4	**46.3**	**82.8**
	All	QRF	**669.6**	**1542.7**	41.2	79.2	**73.4**	**191.2**	39.9	78.5

https://doi.org/10.5194/hess-2022-377
Preprint. Discussion started: 21 November 2022
© Author(s) 2022. CC BY 4.0 License.

Hydrology and Earth System Sciences
Open Access
Discussions

		PLSTM	558.7	1444.1	**46.1**	**83.3**	84.3	214.2	**59.4**	**84.0**
250	PDIR	QRF	0.88	2.53	**38.32**	**80.57**	**0.12**	**0.43**	82.21	**97.24**
		PLSTM	**0.73**	**2.34**	32.47	75.68	0.14	0.50	**86.76**	96.28
	IEMRG-F	QRF	**1.20**	**3.13**	**65.08**	**94.84**	0.10	**0.35**	**82.21**	93.93
		PLSTM	1.24	3.71	62.77	94.29	**0.09**	0.48	79.86	**94.07**
	GSMaP	QRF	**1.20**	**3.12**	57.07	**92.93**	**0.13**	**0.47**	79.86	**98.62**
		PLSTM	1.26	3.35	**58.29**	92.26	0.13	0.49	**85.38**	97.79
	All	QRF	1.11	**2.88**	**60.87**	**93.89**	0.09	**0.33**	80.14	97.38
		PLSTM	**1.00**	3.22	55.30	92.53	**0.08**	0.42	**81.52**	**97.93**

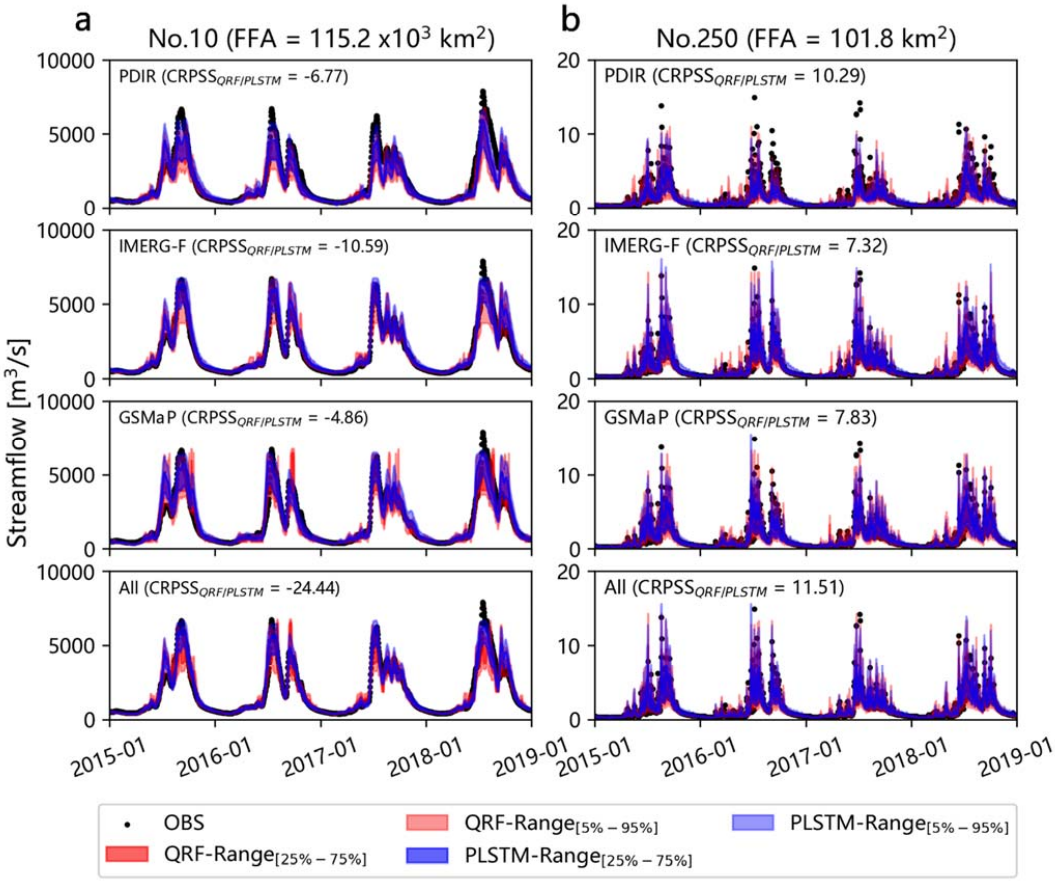

https://doi.org/10.5194/hess-2022-377
Preprint. Discussion started: 21 November 2022
© Author(s) 2022. CC BY 4.0 License.

Figure 9. Hydrographs and prediction intervals for two typical sub-basins. The CRPSS is greater than 0, indicating that the QRF model is better than the PLSTM model; conversely, the PLSTM model is better than the QRF model. OBS in figure indicates streamflow reference. PDIR is a near real-time product; IMERG-F and GSMAP are bias-adjusted products.

4.3 Deterministic (single-point) assessment

Although the post-processing model proposed in this study is probabilistic, decision-makers tend to prefer deterministic (single-point) prediction. Therefore, we utilize the average of the probability members as deterministic predictions to further compare the prediction accuracy of the models. Also, it can be viewed as a Post hoc model examination.

4.3.1 Overall model performance

Figure 10 shows the model performance of the streamflow simulations before post-processing (RAW), and after QRF and PLSTM post-processing for the 522 sub-basins. The metrics shown here include Pearson correlation coefficients (PCC), relative bias (RB), and Nash efficiency coefficients (NSE). Each sub-basin is calculated separately. Also, the means and medians of each metric across all 522 sub-basins are displayed in the first three columns (metric) in Table 4. It can be seen that both QRF and PLSTM are better than RAW, indicating the value of the proposed two post-processing models (Fig.10). For two post-processing models, PLSTM performs better than the QRF model across the board.

https://doi.org/10.5194/hess-2022-377
Preprint. Discussion started: 21 November 2022
© Author(s) 2022. CC BY 4.0 License.

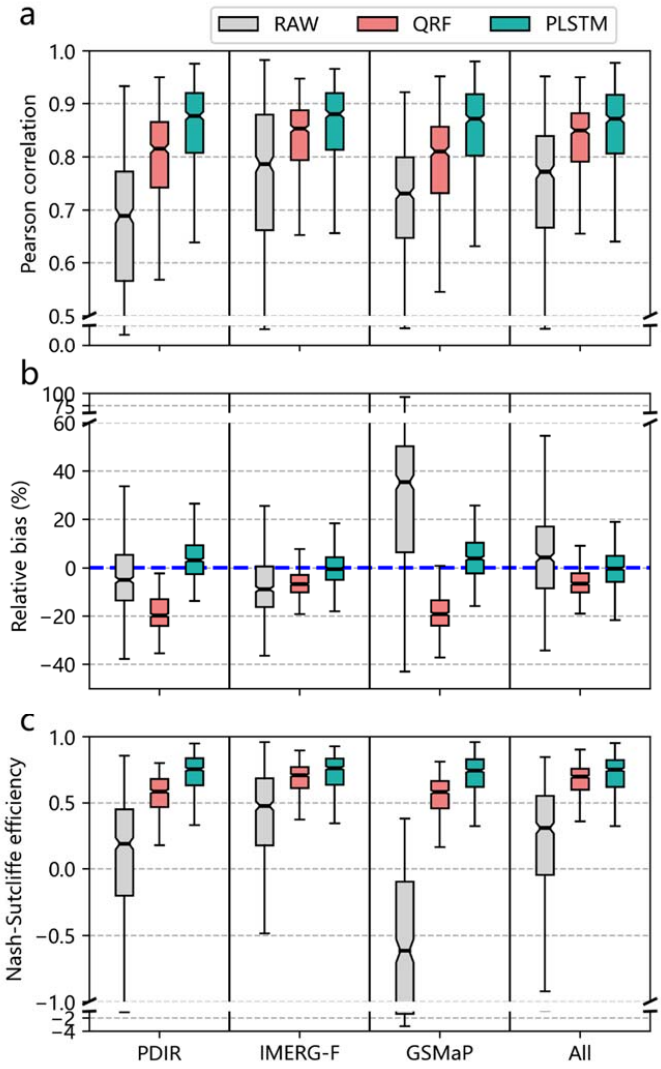

Figure 10. Boxplots of different model performance in 522 sub-basins. (a) Pearson correlation coefficient (PCC); (b) Relative bias (RB); and (c) Nash-Sutcliffe efficiency (NSE). The closer the NSE (PCC) is to 1, the better the model performs. The closer RB is to 0, the better the model performs. Note: PDIR is a near real-time product; IMERG-F and GSMAP are bias-adjusted products.

https://doi.org/10.5194/hess-2022-377
Preprint. Discussion started: 21 November 2022
© Author(s) 2022. CC BY 4.0 License.

4.3.2 Spatial distribution of model performance

Figure 11 shows the spatial characteristics of the Nash-Sutcliffe efficiency (NSE) improvement for streamflow simulations obtained by model comparison. Compared to the raw simulations (RAW), QRF and PLSTM show large enhancements in almost all sub-basins. Among all precipitation-driven streamflow post-processing experiments, PLSTM-GSMaP and QRF-GSMaP provide the most significant improvement in accuracy due to the poorer performance of the raw GSMaP-driven streamflow simulation. On the contrary, the post-processing models bring a smaller improvement in NSE values due to the better performance of the raw IMERG-F-driven streamflow simulations. Even, there is a slight regression in model performance in some sporadic sub-basins. Compared to PLSTM, the QRF model does not show its advantage of deterministic (single-point) estimation and is inferior to the PLSTM model in almost all sub-basins. The largest difference in model performance occurs in GSMaP, followed by PDIR, IMERG-F and multi-model (All). This indicates that the deterministic (single-point) estimation capability of the QRF model differs more from PLSTM for streamflow with poor raw simulation.

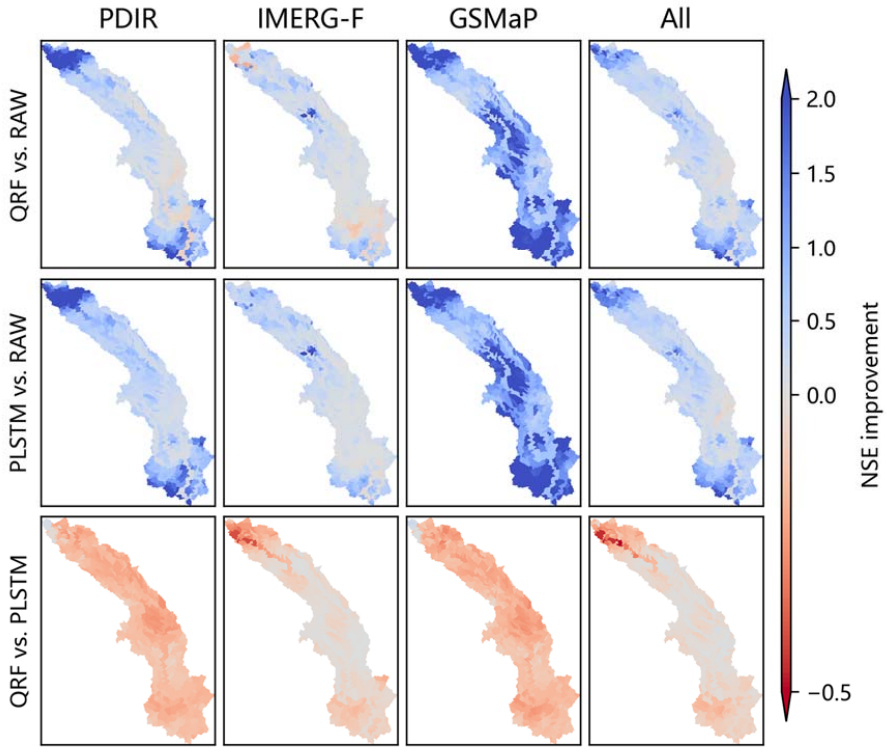

https://doi.org/10.5194/hess-2022-377
Preprint. Discussion started: 21 November 2022
© Author(s) 2022. CC BY 4.0 License.

Figure 11. Individual sub-basin spatial Nash-Sutcliffe efficiency (NSE) improvement between (a) QRF and RAW, (b) PLSTM and RAW and (c) QRF and PLSTM in 522 sub-basins. Blue indicates sub-basins where the former model is better than the latter one, and red indicates sub-basins where the former model is worse than the latter one. The darker the color, the greater the difference. is a near real-time product; IMERG-F and GSMAP are bias-adjusted products.

4.3.3 Model difference between FFAs

Similar to the analysis route in Fig. 6, based on the spatial distribution (Fig. 11), we further explore the relationship between the model performance and the flow accumulation area (FAA) of the sub-basin, and the results are shown in Fig. 12. As the flow accumulation area (FAA) of the sub-basin increases, the model performance also improves. From Fig. 12a, the same conclusion as Fig. 11 can be drawn, PLSTM is better than QRF. Especially when the flow accumulation area (FAA) of the sub-basin is more than 20,000 km^2. The blue points (PLSTM) are distributed on top of the red points (QRF), and the red points are distributed on top of the black points (RAW). It can be seen from Fig. 12b that 20,000 km^2 is also a threshold condition. When the flow accumulation area (FAA) of the sub-basin is larger than the threshold, the gap between PLSTM and QRF is narrowing as the FAA increases. This is most evident in IMERG-F-driven experiments. But for GSMaP, the increase of FAA has little effect on the gap between PLSTM and QRF. This suggests that highly biased information from raw streamflow simulation has a greater impact on the QRF than on the PLSTM model.

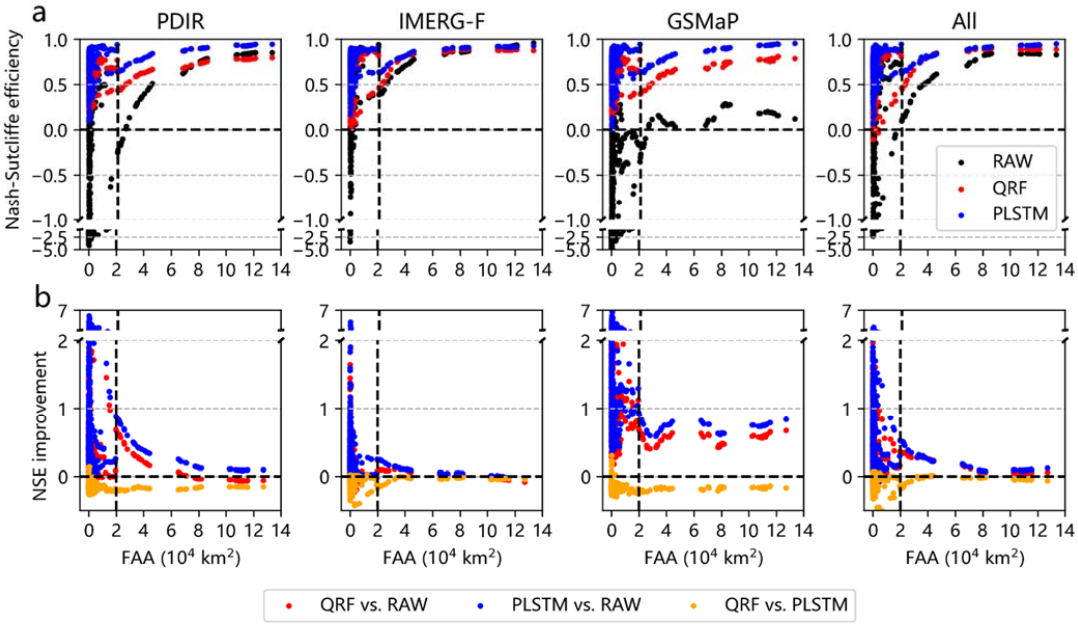

Figure 12. The relationships between (a) Nash-Sutcliffe efficiency (NSE), (b) NSE improvement and flow accumulation area (FAA). The closer the NSE is to 1, the better the model performs. The NSE improvement larger than 0 indicates the former model is better than the

https://doi.org/10.5194/hess-2022-377
Preprint. Discussion started: 21 November 2022
© Author(s) 2022. CC BY 4.0 License.

latter one, conversely, the former model is worse than the latter one. PDIR is a near real-time product; IMERG-F and GSMAP are bias-adjusted products.

4.3.4 High-flow, low-flow, and peak timing

Table 4 summarizes the means and medians of integrated metrics and flow regime indicators of different models in 522 sub-basins. The first three columns are the same as the metrics used in Fig. 10. Pearson correlation coefficient (PCC) and Relative bias (RB) can also be regarded as the components of Nash-Sutcliffe efficiency (NSE). In order to guarantee the robustness of the results, we also calculated another integrated indicator KGE. The KGE performed identically to NSE, confirming the superiority of the PLSTM model.

Table 4. Summary of integrated metrics and flow regime indicators of different models in 522 sub-basins. The bold numbers indicate better performance in each group.

Input	Aggregation	Model	Metric							
			PCC	RB	NSE	KGE	FHV	FMS	FLV	PT
PDIR	Mean	RAW	0.656	**-0.02**	-0.1	0.521	33.11	-5.3	-17.3	1.68
		QRF	0.785	-0.19	0.558	0.621	-43.4	-9.85	**3.143**	1.441
		PLSTM	**0.851**	0.032	**0.712**	**0.755**	**-28.8**	**1.201**	15.24	**1.328**
	Median	RAW	0.689	-0.05	0.19	0.572	**24.77**	-7.63	-12.5	1.692
		QRF	0.815	-0.2	0.584	0.645	-44.6	-10.5	**9.833**	1.417
		PLSTM	**0.877**	**0.032**	**0.752**	**0.778**	-29.6	**0.978**	19.13	**1.273**
IMERG-F	Mean	RAW	0.759	-0.06	0.389	0.664	**10.92**	-4.04	-14.3	1.459
		QRF	0.808	-0.06	0.648	0.718	-35.3	4.268	**-4.29**	1.394
		PLSTM	**0.852**	**-0.01**	**0.715**	**0.765**	-30.4	**2.409**	-5.05	**1.282**
	Median	RAW	0.785	-0.09	0.475	0.672	**9.555**	-6.35	-4.14	1.417
		QRF	0.852	-0.07	0.706	0.739	-37.6	**2.068**	5.878	1.333
		PLSTM	**0.88**	**-0.01**	**0.761**	**0.788**	-32.1	2.159	**2.467**	**1.231**
GSMaP	Mean	RAW	0.687	0.286	-0.92	0.308	88.82	8.465	-45.1	1.519
		QRF	0.778	-0.19	0.545	0.61	-45.4	-11.2	**15.94**	1.703
		PLSTM	**0.848**	**0.043**	**0.703**	**0.741**	**-31.2**	**0.708**	23.71	**1.44**
	Median	RAW	0.731	0.352	-0.62	0.393	82.86	12.08	-34.1	1.5
		QRF	0.809	-0.19	0.579	0.633	-48	-11.1	**23.73**	1.696
		PLSTM	**0.871**	**0.04**	**0.742**	**0.762**	**-32.3**	**1.037**	26.36	**1.417**
All	Mean	RAW	0.733	0.059	0.154	0.603	34.38	**2.332**	-15.5	1.456
		QRF	0.803	-0.06	0.637	0.704	-38.8	3.494	**8.635**	1.532
		PLSTM	**0.846**	**-0.01**	**0.703**	**0.76**	**-32.3**	4.855	10.27	**1.44**
	Median	RAW	0.771	0.042	0.306	0.664	**30.53**	2.228	**-4.74**	1.417
		QRF	0.849	-0.07	0.695	0.727	-42.3	**1.317**	14.96	1.542
		PLSTM	**0.871**	**-0.003**	**0.749**	**0.781**	-33.8	4.436	13.83	**1.417**

https://doi.org/10.5194/hess-2022-377
Preprint. Discussion started: 21 November 2022
© Author(s) 2022. CC BY 4.0 License.

The last four columns are flow-related indicators. Overall, the PLSTM model is still the best, except for the low-flow bias (FLV). The QRF model is the best model for simulating low flow. Nonetheless, as can be seen from the high-flow bias (FHV), both the two post-processing models are limited in their ability to handle flood peaks. Regardless of the streamflow simulations driven by either precipitation product, the bias of the flood peak changes from an overestimation (RAW) to an underestimation (Post-processing). In addition, there is a certain degree of deviation in the simulations of peak time. Flood peaks have always been a challenging problem in hydrological simulation, which also confirms the necessity of probabilistic post-processing.

4.3.5 Hydrograph of two typical sub-basins

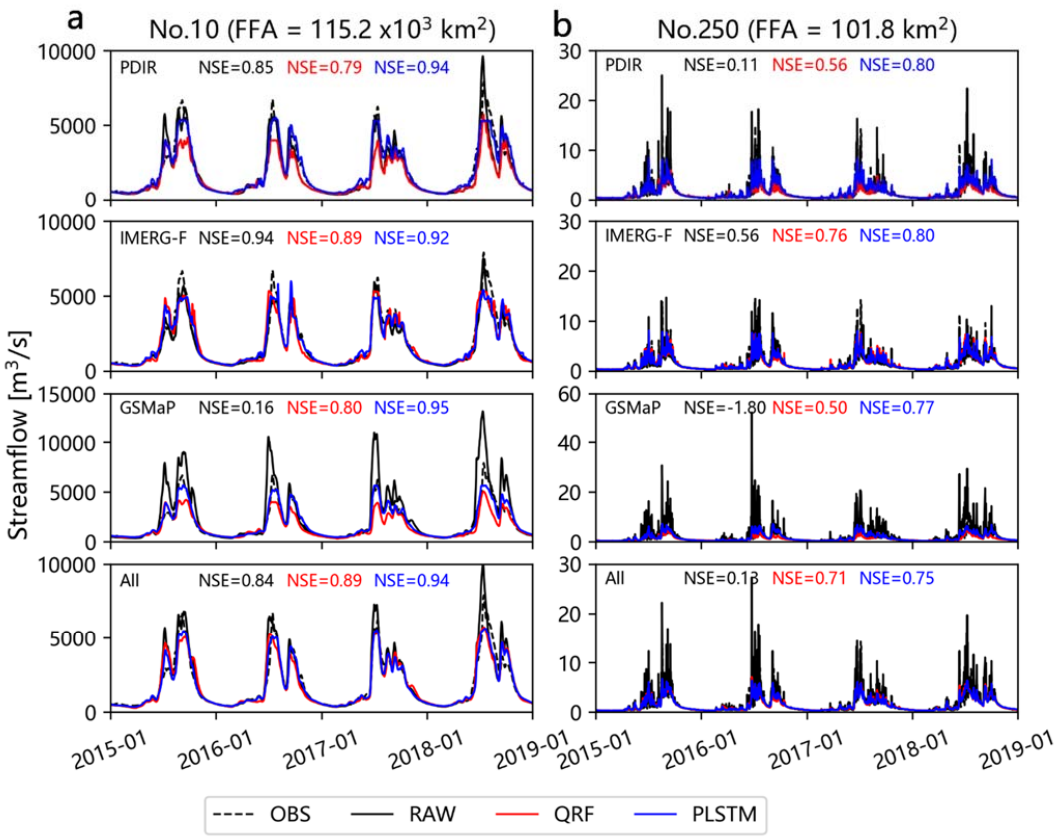

Figure 13. Hydrographs simulated by different models for two typical sub-basins. OBS in figure indicates the streamflow reference. PDIR is a near real-time product; IMERG-F and GSMAP are bias-adjusted products.

https://doi.org/10.5194/hess-2022-377
Preprint. Discussion started: 21 November 2022
© Author(s) 2022. CC BY 4.0 License.

Same as Fig. 9, we still selected the same two typical sub-basins to compare the deterministic post-processing ability of different models (Fig. 13). For the uncorrected runoff simulations (RAW), except for the performance of the IMERG-F product in sub-basin No.10, the other precipitation-driven simulations present overestimation in both sub-basins, which also contributed to the poor NSE values. After QRF and PLSTM post-processing, the streamflow simulation performance is significantly improved. But it also causes an underestimation of the flood peak. Compared with PLSTM, the QRF model underestimates the flood peak more severely. This is also the main reason why the QRF model is inferior to the PLSTM model. It is also consistent with the high flow simulation bias in Table 4.

5 Discussion

5.1 Simulated and observed streamflow reference

Unlike previous studies, the post-processing in this study is for subbasin-scale streamflow from 522 sub-basins in a nested basin. Their flow accumulation areas (FAAs) range from 100 km^2 to 120,000 km^2. In order to perform the streamflow post-processing for the 522 sub-basins, the corresponding streamflow observation should be obtained. However such data are not available. Therefore we use the streamflow simulations from the calibrated hydrological model driven by observed precipitation. In fact, by doing so, the best post-processing model performance can only be infinitely close to the given reference. So, the post-processing we do is an imitation of the streamflow reference. This is not exactly consistent with the post-processing of the real streamflow. However, what we have done is use the generated reference to test the performance of post-processing models. Thus doing so also accomplished our goal. In future studies, the performance of the different post-processing models can be fully compared in more informative basins. However, we believe that our dataset is also very rare in the current community, so we make it open along with this study to allow other researchers to test different algorithms using the same dataset and compare it to the benchmark of this study (Zhang et al., 2022b).

5.2 Model comparison in this study

In this study, we compared two probabilistic post-processing models, the PLSTM and the QRF models. The QRF model is representative of traditional machine learning algorithms based on decision trees and ensemble learning. The PLSTM model was chosen based on the CMAL-LSTM model, proposed by Klotz et al. (2022). In their study, the CMAL-LSTM model achieved the best model performance, which is why we chose it. They also selected two other mixture density networks and a Monte Carlo dropout-based probabilistic method. Besides, there are some other probabilistic forecasting methods, such as variational inference methods (Li et al., 2021), and GANs methods (Pan et al., 2021). It is unrealistic to compare all methods in one study. In a growing community, new methods can be incorporated to brainstorm and continuously improve the performance of post-processing models in future studies.

Another thing that may affect the robustness of the results is the imbalance in the number of sub-basins. A flow accumulation area (FAA) of 60,000 km^2 is a threshold condition in the 522 sub-basins we studied. Above and below 60,000

https://doi.org/10.5194/hess-2022-377
Preprint. Discussion started: 21 November 2022
© Author(s) 2022. CC BY 4.0 License.

km^2, there is a large difference in model performance between the two probabilistic post-processing models. However, among the 522 sub-basins selected, only 27 sub-basins (5.2%) have a flow accumulation area (FAA) greater than 60,000 km^2, while all other sub-basins (94.8%) have a flow accumulation area (FAA) less than 60,000 km^2. This may affect the robustness of the results, such as more discrete scatters in the reliability diagrams (Fig. 5). The comparison of the PLSTM and QRF models in a larger number and more balanced basins can further increase the robustness of our results as well as improve our understanding of the different post-processing models (Kratzert et al., 2022b).

5.3 Global model and local model

In previous studies using the LSTM model, the best practice obtained is the global LSTM model. That is, one LSTM model is used for all data sets and the entire study area. The results of these studies show that the global LSTM model performs better than the local model (Kratzert et al., 2019b; Fang et al., 2022). Moreover, the global LSTM model is able to achieve good results in ungauged basins (Kratzert et al., 2019a). In our study, we aim at streamflow probabilistic post-processing in 522 sub-basins. In the process of PLSTM to generate probabilistic outputs, for the robustness of the results, we first randomly sample 10,000 times in each basin and at each time step, and then obtain the final probabilistic members after taking 100 quantiles. For 522 sub-basins, a total of 522×4×365×10000 = 7,621,200,000 samples are required for a 4-year test period. We used a single-card RTX3090 GPU with 24G of video memory for this study, but the amount of sampling required is much larger than the memory of our device. We therefore chose to train a local model for each sub-basin in this study. Future comparisons of the global and local models can be tested on devices with enough video memory, such as clusters or supercomputers containing multi-card GPUs. However, for post-processing in ungauged basins, Frame et al. (2021) give us the insight that the global LSTM model may give poorer post-processing results in these areas. This is due to the effect of basin area and flow regime. Therefore, for the objective of this study, post-processing uncorrected precipitation-driven streamflow simulations, the performance of the global model may be more influenced by the spatial distribution of biases.

5.4 Predictors or input features

In order to keep the model complexity and computational cost low, the predictor selected for this study is only one variable, the streamflow. However, more variables are available as predictors, including other meteorological variables, such as temperature and wind speed (Frame et al., 2021). These variables are also used to force hydrological models (Jiang et al., 2022). In addition, basin attributes are important predictors, especially in the global model. In previous studies, all of these variables have been shown to help the model to vary degrees (Jiang et al., 2022). For post-processing, there are also studies that use model state variables and other output variables as predictors for experiments (Frame et al., 2021). Basins-related attributes can provide us with local information, which is particularly helpful for simulations in ungauged areas. State variables or other output variables can give us information about the hydrological model, which also be considered as hybrid modeling. This increases the physical interpretability of the post-processing framework (Razavi, 2021; Tsai et al., 2021). However, biased

https://doi.org/10.5194/hess-2022-377
Preprint. Discussion started: 21 November 2022
© Author(s) 2022. CC BY 4.0 License.

precipitation-driven hydrologic models generate state variables and outputs that are often biased as well. Whether this is helpful for streamflow post-processing is unknown and needs to be further explored.

5.5 Predictors or input features

In this study, only a single hydrological model (DTVGM) is used to simulate streamflow obtained from different precipitation drivers to increase the diversity of post-processing experiments. Also, this excludes other two uncertainty sources, e.g., model structure and parameters. Therefore, the present study focuses on post-processing model comparisons for input uncertainties. In addition to input uncertainty, hydrologic model structure and parameter uncertainty are also important sources of uncertainty (Herrera et al., 2022; Mai et al., 2022). Future post-processing model comparisons can be performed using a multiple hydrological model approach to analyze model structure and model parameter uncertainties (Ghiggi et al., 2021; Troin et al., 2021; Mai et al., 2022).

5.6 Extreme events

Through comparative analysis and visualization, it can be found that both PLSTM and QRF models have some limitations in handling extreme events. Even, the QRF model performs a bit worse. This is because the QRF model is based on decision trees. The model prediction is performed by a historical analogy search. That is, the random forests model first finds the most similar samples in the training samples, and then the similar samples of the leaf nodes of multiple decision trees are averaged to obtain the final predictions (Li and Martin, 2017). There is no doubt that the limited sample, especially for extreme events, determines that it is not able to solve the prediction of extreme events very well. Not to mention that for post-processing extreme events that have never happened in history, the nature of QRF dictates that it is powerless. Fortunately, this can be improved by introducing extra parametric hybrid methods (e.g., a mix of RF and extreme-value distribution). Attempts that have occurred include a combination of QRF and extended generalized Pareto distributions (Taillardat et al., 2019). However, this class of hybrid approaches introduces additional complexity to the model and more hyperparameters that need to be calibrated. The PLSTM model is also limited by the sample size of extreme events, but it outperforms the QRF model in terms of these extreme events. It is a sign that the deep neural network is stronger than the decision tree class of traditional machine learning models. Compared to the historical analogy search of the QRF model, the LSTM model is able to make "true" predictions by neuronal computation based on predictors. And, the PLSTM model chosen in this study belongs directly to the mixture density networks. Their parameters are learned directly by neural network optimization (e.g., gradient descent algorithm). We believe this can be further improved by introducing more predictors and other distribution functions that are more specific to extreme events.

https://doi.org/10.5194/hess-2022-377
Preprint. Discussion started: 21 November 2022
© Author(s) 2022. CC BY 4.0 License.

5 Conclusions

We conduct a series of well-designed experiments comparing a machine learning model (quantile regression forests, QRF) and a deep learning model (probabilistic long short-term memory network, PLSTM) for streamflow probabilistic post-processing. By driving the calibrated hydrological model with observed precipitation and three satellite precipitation products respectively, we generated streamflow reference and biased streamflow simulations, and used them to construct a standard dataset containing 522 sub-basins. Post-processing model performance is fully assessed through probabilistic and deterministic metrics.

In conclusion, decision-tree models based on historical search (including random forest but not limited to it) have limited ability to predict extreme values, but their low complexity and high parallelism makes them more efficient. Deep learning models (including PLSTM but not limited to it) fit the extreme values better by a deeper network. The performance will be stronger when more predictors are fed. But it comes at the cost of more computational resources. Model comparison improves our knowledge and understanding of the models. The use and development of different models requires the user to choose according to their needs and capabilities.

The empirical findings of this study between the two post-processing models are summarized below.

(1) The probabilistic assessment indicates that the QRF and PLSTM models perform comparably. Their model differences are closely related to the flow accumulation area (FAA) of the sub-basin and there is a scale effect. The threshold condition is 60,000 km^2. When the FAA of the sub-basin is less than the threshold, the QRF model performs better than the PLSTM model in most cases. When the FAA of the sub-basin is larger than the threshold, the PLSTM model should be preferred.

(2) The deterministic assessment shows that the PLSTM model outperforms the QRF model. The PLSTM model captures high-flow process and flow duration curve better than the QRF model. The latter tends to underestimate the high-flow process. However, both models underestimate flood peaks due to the problem of sparse samples of extreme events.

(3) For the input uncertainties introduced by the different satellite precipitation products, both models are able to reduce their impact on the streamflow simulation. However, the multi-feature experiments do not further improve the performance of the post-processing models. On the contrary, model performance degrades due to the mixing of highly biased inputs.

The results of both post-processing models and the constructed standard dataset of this study are made available through Zenodo repository (https://zenodo.org/record/7187505) (Zhang et al., 2022b). We expect more models to be compared by standard datasets and eventually enrich the model zoo of hydrological probabilistic post-processing.

Data and code availability. The GPM IMERG Final Run is free available at GES DISC (https://gpm.nasa.gov/node/3328). The PDIR data can be freely download from CHRS Data Portal (http://chrsdata.eng.uci.edu/). The GSMaP data is publicly available (at https://sharaku.eorc.jaxa.jp/GSMaP/index.htm). The CMA precipitation observation is provided by the National Meteorological Information Center of China Meteorological Administration. The soil types are free available at http://www.fao.org/soils-portal/soil-survey/soil-maps-and-databases/harmonized-world-soil-database-v12/en/. The land use

data is free available from Chinese National Tibetan Plateau Third Pole Environment Data Center at http://data.tpdc.ac.cn/en/data/a75843b4-6591-4a69-a5e4-6f94099ddc2d/. The DEM data is free available at https://www.gscloud.cn/. The QRF model code is available at Github repository (https://github.com/jnelson18/pyquantrf) (Jnelson18, 2022). The PLSTM model code is available at Github repository (https://github.com/neuralhydrology/neuralhydrology) (Kratzert et al., 2022a). The dataset and results of this study are available at Zenodo repository (https://zenodo.org/record/7187505) (Zhang et al., 2022b).

Author contribution. Conceptualization, YZ, AY, PN, BA, SS, KH and YW; methodology, YZ and AY; software, YZ and AY; validation, YZ; data curation, YZ, AY, PN and BA; visualization, YZ; supervision, AY KH, and SS; project administration, AY. and SS; funding acquisition, AY and SS. original draft preparation, YZ; review and editing, YZ, AY, PN, BA, SS, KH and YW; All authors have read and agreed to the published version of the manuscript.

Competing interests. The authors declare that they have no conflict of interest.

Acknowledgements. This research is jointly supported by the Natural Science Foundation of China (No. 42171022, 51879009), the Second Tibetan Plateau Scientific Expedition and Research Program (No. 2019QZKK0405), the National Key Research and Development Program of China (No. 2018YFE0196000), the U.S. Department of Energy (DOE Prime Award DE-IA0000018).

References

Althoff, D., Rodrigues, L. N., and Bazame, H. C.: Uncertainty quantification for hydrological models based on neural networks: the dropout ensemble, Stochastic Environmental Research and Risk Assessment, 35(5), 1051-1067, https://doi.org/10.1007/s00477-021-01980-8, 2021.

Beven, K.: Changing ideas in hydrology—the case of physically-based models, Journal of Hydrology, 105(1-2), 157-172, https://doi.org/10.1016/0022-1694(90)90161-P, 1989.

Bogner, K., and Pappenberger, F.: Multiscale error analysis, correction, and predictive uncertainty estimation in a flood forecasting system, Water Resources Research, 47(7), e2010WR009137, https://doi.org/10.1029/2010WR009137, 2011.

Bormann, K. J., Evans, J. P., and McCabe, M. F.: Constraining snowmelt in a temperature-index model using simulated snow densities, Journal of Hydrology, 517, 652-667, https://doi.org/10.1016/j.jhydrol.2014.05.073, 2014.

Breiman, L.: Random forests, Machine Learning, 45(1), 5-32, https://doi.org/10.1023/a:1010933404324, 2001.

Bröcker, J.: Evaluating raw ensembles with the continuous ranked probability score, Quarterly Journal of the Royal Meteorological Society, 138(667), 1611-1617, https://doi.org/10.1002/qj.1891, 2012.

Chawanda, C. J., George, C., Thiery, W., Griensven, A. V., Tech, J., Arnold, J., and Srinivasan, R.: User-friendly workflows for catchment modelling: Towards reproducible SWAT+ model studies, Environmental Modelling and Software, 134, 104812, https://doi.org/10.1016/j.envsoft.2020.104812, 2020.

Chen, H., Yong, B., Shen, Y., Liu, J., Hong, Y., and Zhang, J.: Comparison analysis of six purely satellite-derived global precipitation estimates, Journal of Hydrology, 581, 124376, https://doi.org/10.1016/j.jhydrol.2019.124376, 2020.

Clark, M. P., Nijssen, B., Lundquist, J. D., Kavetski, D., Rupp, D. E., Woods, R. A., Freer, J. E., Gutmann, E. D., Wood, A. W., Brekke, L. D., Arnold, J. R., Gochis, D. J., and Rasmussen, R. M.: A unified approach for process-based hydrologic modeling: 1. Modeling concept, Water Resources Research, 51(4), 2498-2514, https://doi.org/10.1002/2015WR017198, 2015.

Corzo Perez, G. A., Van Huijgevoort, M., Voß, F., and Van Lanen, H.: On the spatio-temporal analysis of hydrological droughts from global hydrological models, Hydrology and Earth System Sciences, 15(9), 2963-2978, https://doi.org/10.5194/hessd-8-619-2011, 2011.

Cunha, L. K., Mandapaka, P. V., Krajewski, W. F., Mantilla, R., and Bradley, A. A.: Impact of radar-rainfall error structure on estimated flood magnitude across scales: An investigation based on a parsimonious distributed hydrological model, Water Resources Research, 48(10), https://doi.org/10.1029/2012WR012138, 2012.

Dembélé, M., Hrachowitz, M., Savenije, H. H. G., Mariéthoz, G., and Schaefli, B.: Improving the Predictive Skill of a Distributed Hydrological Model by Calibration on Spatial Patterns With Multiple Satellite Data Sets, Water Resources Research, 56(1), https://doi.org/10.1029/2019WR026085, 2020.

Dong, J., Crow, W. T., and Reichle, R.: Improving Rain/No-Rain Detection Skill by Merging Precipitation Estimates from Different Sources, Journal of Hydrometeorology, 21(10), 2419-2429. https://doi.org/10.1175/JHM-D-20-0097.1, 2020.

Evin, G., Lafaysse, M., Taillardat, M., and Zamo, M.: Calibrated ensemble forecasts of the height of new snow using quantile regression forests and ensemble model output statistics, Nonlinear Processes in Geophysics, 28(3), 467-480, https://doi.org/10.5194/npg-28-467-2021, 2021.

Falck, A. S., Maggioni, V., Tomasella, J., Vila, D. A., and Diniz, F. L. R.: Propagation of satellite precipitation uncertainties through a distributed hydrologic model: A case study in the Tocantins–Araguaia basin in Brazil, Journal of Hydrology, 527, 943-957, https://doi.org/10.1016/j.jhydrol.2015.05.042, 2015.

Fang, K., and Shen, C.: Near-Real-Time Forecast of Satellite-Based Soil Moisture Using Long Short-Term Memory with an Adaptive Data Integration Kernel, Journal of Hydrometeorology, 21(3), 399-413, https://doi.org/10.1175/JHM-D-19-0169.1, 2020.

Fang, K., Kifer, D., Lawson, K., Feng, D., and Shen, C.: The data synergy effects of time-series deep learning models in hydrology, Water Resources Research, e2021WR029583. https://doi.org/10.1029/2021WR029583, 2022.

Fang, K., Shen, C., Kifer, D., and Yang, X.: Prolongation of SMAP to spatiotemporally seamless coverage of continental US using a deep learning neural network, Geophysical Research Letters, 44(21), 11-30, https://doi.org/10.1002/2017GL075619, 2017.

© Author(s) 2022. CC BY 4.0 License.

Frame, J. M., Kratzert, F., Raney, A., Rahman, M., Salas, F. R., and Nearing, G. S.: Post-Processing the National Water Model with Long Short-Term Memory Networks for Streamflow Predictions and Model Diagnostics, JAWRA Journal of the American Water Resources Association, 57(6), 885-905, https://doi.org/10.1111/1752-1688.12964, 2021.

Ghiggi, G., Humphrey, V., Seneviratne, S. I., and Gudmundsson, L.: G-RUN ENSEMBLE: A Multi-Forcing Observation-Based Global Runoff Reanalysis, Water Resources Research, 57(5), e2020WR028787, https://doi.org/10.1029/2020WR028787, 2021.

Gneiting, T., Balabdaoui, F., and Raftery, A. E.: Probabilistic forecasts, calibration and sharpness, Journal of the Royal Statistical Society: Series B (Statistical Methodology), 69(2), 243-268, https://doi.org/10.1111/j.1467-9868.2007.00587.x, 2007.

Gou, J., Miao, C., Duan, Q., Tang, Q., Di, Z., Liao, W., Wu, J., and Zhou, R.: Sensitivity Analysis-Based Automatic Parameter Calibration of the VIC Model for Streamflow Simulations Over China, Water Resources Research, 56(1), e2019WR025968, https://doi.org/10.1029/2019WR025968, 2020.

Gou, J., Miao, C., Samaniego, L., Xiao, M., Wu, J., and Guo, X.: CNRD v1.0: A High-Quality Natural Runoff Dataset for Hydrological and Climate Studies in China. Bulletin of the American Meteorological Society, 102(5), E929-E947. https://doi.org/10.1175/BAMS-D-20-0094.1, 2021.

Hartmann, H. C., Pagano, T. C., Sorooshian, S., and Bales, R.: Confidence builders: Evaluating seasonal climate forecasts from user perspectives, Bulletin of the American Meteorological Society, 83(5), 683-698, https://doi.org/10.1175/1520-0477(2002)083<0683:CBESCF>2.3.CO;2, 2002.

Herrera, P. A., Marazuela, M. A., and Hofmann, T.: Parameter estimation and uncertainty analysis in hydrological modelling, Wiley Interdisciplinary Reviews-Water, 9(1), e1569, https://doi.org/10.1002/wat2.1569, 2022.

Honti, M., Scheidegger, A., and Stamm, C.: The importance of hydrological uncertainty assessment methods in climate change impact studies, Hydrology and Earth System Sciences, 18(8), 3301-3317, https://doi.org/10.5194/hess-18-3301-2014, 2014.

Hori, T., Cho, J., and Watanabe, S.: End-to-end speech recognition with word-based RNN language models, 2018 IEEE Spoken Language Technology Workshop (SLT), 389-396, https://doi.org/10.1109/SLT.2018.8639693, 2018.

Hou, A. Y., Kakar, R. K., Neeck, S., AA, A., Kummerow, C. D., Kojima, M., Oki, R., Nakamura, K., and Iguchi, T.: The Global Precipitation Measurement Mission, Bulletin of the American Meteorological Society, 95(5), 701-722, https://doi.org/10.1175/BAMS-D-13-00164.1, 2013.

Huffman, G. J., Bolvin, D. T., Nelkin, E. J., and Tan, J.: Integrated Multi-satellitE Retrievals for GPM (IMERG) technical documentation, NASA/GSFC Code, 612(47), 2019, 2015.

Huffman, G.J., E.F. Stocker, D.T. Bolvin, E.J. Nelkin, Jackson T.: GPM IMERG Final Precipitation L3 1 day 0.1 degree x 0.1 degree V06, Edited by Andrey Savtchenko, Greenbelt, MD, Goddard Earth Sciences Data and Information Services Center (GES DISC), Accessed: [2021-7-30], https://doi.org/10.5067/GPM/IMERGDF/DAY/06, 2019.

Jajarmizadeh, M., Harun, S., and Salarpour, M.: A review on theoretical consideration and types of models in hydrology, Journal of Environmental Science and Technology, 5(5), 249-261, https://doi.org/10.3923/jest.2012.249.261, 2012.

Jiang, L., and Bauer-Gottwein, P.: How do GPM IMERG precipitation estimates perform as hydrological model forcing? Evaluation for 300 catchments across Mainland China, Journal of Hydrology, 572, 486-500, https://doi.org/10.1016/j.jhydrol.2019.03.042, 2019.

Jiang, S., Zheng, Y., Wang, C., and Babovic, V.: Uncovering Flooding Mechanisms Across the Contiguous United States Through Interpretive Deep Learning on Representative Catchments, Water Resources Research, 58(1), e2021WR030185, https://doi.org/10.1029/2021WR030185, 2022.

Jnelson18.: jnelson18/pyquantrf: DOI release (v0.0.3doi), Zenodo [code], https://doi.org/10.5281/zenodo.5815105, 2022.

Kasraei, B., Heung, B., Saurette, D. D., Schmidt, M. G., Bulmer, C. E., and Bethel, W.: Quantile regression as a generic approach for estimating uncertainty of digital soil maps produced from machine-learning, Environmental Modelling and Software, 144, 105139, https://doi.org/10.1016/j.envsoft.2021.105139, 2021.

Kaune, A., Chowdhury, F., Werner, M., and Bennett, J.: The benefit of using an ensemble of seasonal streamflow forecasts in water allocation decisions, Hydrology and Earth System Sciences, 24(7), 3851-3870, https://doi.org/10.5194/hess-24-3851-2020, 2020.

Khakbaz, B., Imam, B., Hsu, K., and Sorooshian, S.: From lumped to distributed via semi-distributed: Calibration strategies for semi-distributed hydrologic models, Journal of Hydrology, 418, 61-77. https://doi.org/10.1016/j.jhydrol.2009.02.021, 2012.

Kling, H., Fuchs, M., and Paulin, M.: Runoff conditions in the upper Danube basin under an ensemble of climate change scenarios, Journal of Hydrology, 424, 264-277, https://doi.org/10.1016/j.jhydrol.2012.01.011, 2012.

Klotz, D., Kratzert, F., Gauch, M., Keefe Sampson, A., Brandstetter, J., Klambauer, G., Hochreiter, S., and Nearing, G.: Uncertainty estimation with deep learning for rainfall–runoff modelling, Hydrology and Earth System Sciences, 26(6), 1673-1693, https://doi.org/10.5194/hess-26-1673-2022, 2022.

Kobold, M., and Sušelj, K.: Precipitation forecasts and their uncertainty as input into hydrological models, Hydrology and Earth System Sciences, 9(4), 322-332, https://doi.org/10.5194/hess-9-322-2005, 2005.

Kratzert, F., Klotz, D., Brenner, C., Schulz, K., and Herrnegger, M.: Rainfall–runoff modelling using Long Short-Term Memory (LSTM) networks, Hydrology and Earth System Sciences, 22(11), 6005-6022, https://doi.org/10.5194/hess-22-6005-2018, 2018.

Kratzert, F., Klotz, D., Herrnegger, M., Sampson, A. K., Hochreiter, S., and Nearing, G. S.: Toward Improved Predictions in Ungauged Basins: Exploiting the Power of Machine Learning, Water Resources Research, 55(12), 11344-11354, https://doi.org/10.1029/2019WR026065, 2019a.

Kratzert, F., Klotz, D., Hochreiter, S., and Nearing, G. S.: A note on leveraging synergy in multiple meteorological data sets with deep learning for rainfall–runoff modelling, Hydrology and Earth System Sciences, 25(5), 2685-2703, https://doi.org/10.5194/hess-25-2685-2021, 2021.

Kratzert, F., Klotz, D., Shalev, G., Klambauer, G., Hochreiter, S., and Nearing, G.: Towards learning universal, regional, and local hydrological behaviors via machine learning applied to large-sample datasets, Hydrology and Earth System Sciences, 23(12), 5089-5110, https://doi.org/10.5194/hess-23-5089-2019, 2019b.

Kratzert, F., Gauch, M., Nearing, G., and Klotz, D.: NeuralHydrology-A Python library for Deep Learning research in hydrology, Journal of Open Source Software, 7(71), 4050, https://doi.org/10.21105/joss.04050, 2022a

Kratzert, F., Nearing, G., Addor, N., Erickson, T., Gauch, M., Gilon, O., Gudmundsson, L., Hassidim, A., Klotz, D., and Nevo, S.: Caravan-A global community dataset for large-sample hydrology, EarthArXiv, [preprint], https://doi.org/10.31223/X50S70, 2022b.

Kubota, T., Aonashi, K., Ushio, T., Shige, S., Takayabu, Y. N., Kachi, M., Arai, Y., Tashima, T., Masaki, T., and Kawamoto, N.: Global Satellite Mapping of Precipitation (GSMaP) products in the GPM era, Satellite precipitation measurement, 1, 355-373, https://doi.org/10.1007/978-3-030-24568-9_20, 2020.

Kubota, T., Shige, S., Hashizume, H., Aonashi, K., Takahashi, N., Seto, S., Hirose, M., Takayabu, Y. N., Ushio, T., and Nakagawa, K.: Global precipitation map using satellite-borne microwave radiometers by the GSMaP project: Production and validation, IEEE Transactions On Geoscience and Remote Sensing, 45(7), 2259-2275, https://doi.org/10.1109/TGRS.2007.895337, 2007.

Lees, T., Buechel, M., Anderson, B., Slater, L., Reece, S., Coxon, G., and Dadson, S. J.: Benchmarking Data-Driven Rainfall-Runoff Models in Great Britain: A comparison of LSTM-based models with four lumped conceptual models, Hydrology and Earth System Sciences, 25(10), 5517–5534, https://doi.org/10.5194/hess-2021-127, 2021.

Li, A. H., and Martin, A.: Forest-type regression with general losses and robust forest, Proceedings of the 34th International Conference on Machine Learning, 70, 2091-2100, 2017.

Li, B., Friedman, J., Olshen, R., and Stone, C.: Classification and regression trees (CART), Biometrics, 40(3), 358-361, Retrieved from http://statweb.lsu.edu/faculty/li/IIT/tree1.pdf, 1984.

Li, D., Marshall, L., Liang, Z., and Sharma, A.: Hydrologic multi-model ensemble predictions using variational Bayesian deep learning, Journal of Hydrology, 604, 127221, https://doi.org/10.1016/j.jhydrol.2021.127221, 2022.

Li, D., Marshall, L., Liang, Z., Sharma, A., and Zhou, Y., Bayesian LSTM With Stochastic Variational Inference for Estimating Model Uncertainty in Process-Based Hydrological Models, Water Resources Research, 57(9), https://doi.org/10.1029/2021WR029772, 2021.

Li, M., Wang, Q. J., Bennett, J. C., and Robertson, D. E.: A strategy to overcome adverse effects of autoregressive updating of streamflow forecasts, Hydrology and Earth System Sciences, 19(1), 1-15, https://doi.org/10.5194/hess-19-1-2015, 2015.

Li, M., Wang, Q. J., Bennett, J. C., and Robertson, D. E.: Error reduction and representation in stages (ERRIS) in hydrological modelling for ensemble streamflow forecasting, Hydrology and Earth System Sciences, 20(9), 3561-3579, https://doi.org/10.5194/hess-20-3561-2016, 2016.

Li, W., Duan, Q., Miao, C., Ye, A., Gong, W., and Di, Z.: A review on statistical postprocessing methods for hydrometeorological ensemble forecasting, Wiley Interdisciplinary Reviews: Water, 4(6), e1246, https://doi.org/10.1002/wat2.1246, 2017.

Mai, J., Craig, J. R., Tolson, B. A., and Arsenault, R.: The sensitivity of simulated streamflow to individual hydrologic processes across North America, Nature Communications, 13(1), https://doi.org/10.1038/s41467-022-28010-7, 2022.

Mai, J., Shen, H., Tolson, B. A., Gaborit, É., Arsenault, R., Craig, J. R., Fortin, V., Fry, L. M., Gauch, M., Klotz, D., Kratzert, F., O'Brien, N., Princz, D. G., Rasiya Koya, S., Roy, T., Seglenieks, F., Shrestha, N. K., Temgoua, A. G. T., Vionnet, V., and Waddell, J. W.: The Great Lakes Runoff Intercomparison Project Phase 4: the Great Lakes (GRIP-GL), Hydrology and Earth System Sciences, 26(13), 3537-3572, https://doi.org/10.5194/hess-26-3537-2022, 2022.

Meinshausen, N., and Ridgeway, G.: Quantile regression forests, Journal of Machine Learning Research, 7(6), 983-999, https://www.jmlr.org/papers/volume7/meinshausen06a/meinshausen06a.pdf, 2006.

Miao, C., Gou, J., Fu, B., Tang, Q., Duan, Q., Chen, Z., Lei, H., Chen, J., Guo, J., and Borthwick, A. G.: High-quality reconstruction of China's natural streamflow, Science Bulletin, 67(5), 547-556, https://doi.org/10.1016/j.scib.2021.09.022, 2022.

Nash, J. E., and Sutcliffe, J. V.: River flow forecasting through conceptual models part I—A discussion of principles, Journal of Hydrology, 10(3), 282-290, https://doi.org/10.1016/0022-1694(70)90255-6, 1970.

Nasreen, S., Součková, M., Vargas Godoy, M. R., Singh, U., Markonis, Y., Kumar, R., Rakovec, O., and Hanel, M.: A 500-year runoff reconstruction for European catchments, Earth System Science Data, 14, 4035–4056, https://doi.org/10.5194/essd-14-4035-2022, 2022.

Nearing, G. S., Tian, Y., Gupta, H. V., Clark, M. P., Harrison, K. W., and Weijs, S. V.: A philosophical basis for hydrological uncertainty, Hydrological sciences journal, 61(9), 1666-1678, https://doi.org/10.1080/02626667.2016.1183009, 2016.

Nguyen, P., Ombadi, M., Gorooh, V. A., Shearer, E. J., Sadeghi, M., Sorooshian, S., Hsu, K., Bolvin, D., and Ralph, M. F.: PERSIANN Dynamic Infrared–Rain Rate (PDIR-Now): A Near-Real-Time, Quasi-Global Satellite Precipitation Dataset, Journal of Hydrometeorology, 21(12), 2893-2906, https://doi.org/10.1175/JHM-D-20-0177.1, 2020a.

Nguyen, P., Shearer, E. J., Ombadi, M., Gorooh, V. A., Hsu, K., Sorooshian, S., Logan, W. S., and Ralph, M.: PERSIANN Dynamic Infrared–Rain Rate Model (PDIR) for High-Resolution, Real-Time Satellite Precipitation Estimation, Bulletin of the American Meteorological Society, 101(3), E286-E302, https://doi.org/10.1175/BAMS-D-19-0118.1, 2020b.

Pan, B., Anderson, G. J., Goncalves, A., Lucas, D. D., Bonfils, C. J., Lee, J., Tian, Y., and Ma, H. Y.: Learning to correct climate projection biases, Journal of Advances in Modeling Earth Systems, 13(10), e2021MS002509, https://doi.org/10.1029/2021MS002509, 2021.

Parrish, M. A., Moradkhani, H., and DeChant, C. M.: Toward reduction of model uncertainty: Integration of Bayesian model averaging and data assimilation, Water Resources Research, 48(3), https://doi.org/10.1029/2011WR011116, 2012.

Razavi, S.: Deep learning, explained: Fundamentals, explainability, and bridgeability to process-based modelling, Environmental Modelling and Software, 144, 105159, https://doi.org/10.1016/j.envsoft.2021.105159, 2021.

Schaake, J. C., Hamill, T. M., Buizza, R., and Clark, M.: HEPEX: the hydrological ensemble prediction experiment, Bulletin of the American Meteorological Society, 88(10), 1541-1548, https://doi.org/10.1175/BAMS-88-10-1541, 2007.

Shen, C., and Lawson, K.: Applications of deep learning in hydrology, Deep Learning for the Earth Sciences: A Comprehensive Approach to Remote Sensing, Climate Science, and Geosciences, 283-297, https://doi.org/10.1002/9781119646181.ch19, 2021.

Shen, Y., Ruijsch, J., Lu, M., Sutanudjaja, E. H., and Karssenberg, D.: Random forests-based error-correction of streamflow from a large-scale hydrological model: Using model state variables to estimate error terms, Computers and Geosciences, 159, 105019, https://doi.org/10.1016/j.cageo.2021.105019, 2022.

Shen, Z., Yong, B., Gourley, J. J., and Qi, W.: Real-time bias adjustment for satellite-based precipitation estimates over Mainland China, Journal of Hydrology, 596, 126133, https://doi.org/10.1016/j.jhydrol.2021.126133, 2021.

Sit, M., Demiray, B. Z., Xiang, Z., Ewing, G. J., Sermet, Y., and Demir, I.: A comprehensive review of deep learning applications in hydrology and water resources, Water Science and Technology, 82(12), 2635-2670, https://doi.org/10.2166/wst.2020.369, 2020.

Sittner, W. T., Schauss, C. E., and Monro, J. C.: Continuous hydrograph synthesis with an API-type hydrologic model, Water Resources Research, 5(5), 1007-1022, https://doi.org/10.1029/WR005i005p01007, 1969.

Sivapalan, M.: From engineering hydrology to Earth system science: milestones in the transformation of hydrologic science, Hydrology and Earth System Sciences, 22(3), 1665-1693, https://doi.org/10.5194/hess-22-1665-2018, 2018.

Sordo-Ward, Á., Granados, I., Martín-Carrasco, F., and Garrote, L.: Impact of Hydrological Uncertainty on Water Management Decisions, Water Resources Management, 30(14), 5535-5551, https://doi.org/10.1007/s11269-016-1505-5, 2016.

Staudemeyer, R. C., and Morris, E. R.: Understanding LSTM-a tutorial into long short-term memory recurrent neural networks, arXiv [preprint], arXiv:1909.09586, 2019.

Sun, Q., Miao, C., Duan, Q., Ashouri, H., Sorooshian, S., and Hsu, K. L.: A Review of Global Precipitation Data Sets: Data Sources, Estimation, and Intercomparisons, Reviews of Geophysics, 56(1), 79-107, https://doi.org/10.1002/2017RG000574, 2018.

Taillardat, M., Fougères, A., Naveau, P., and Mestre, O.: Forest-Based and Semiparametric Methods for the Postprocessing of Rainfall Ensemble Forecasting, Weather and Forecasting, 34(3), 617-634, https://dio.org/10.1175/WAF-D-18-0149.1, 2019.

Taillardat, M., Mestre, O., Zamo, M., and Naveau, P.: Calibrated Ensemble Forecasts Using Quantile Regression Forests and Ensemble Model Output Statistics, Monthly Weather Review, 144(6), 2375-2393, https://doi.org/10.1175/MWR-D-15-0260.1, 2016.

Tan, M. L., Gassman, P. W., Yang, X., and Haywood, J.: A review of SWAT applications, performance and future needs for simulation of hydro-climatic extremes, Advances in Water Resources, 143, 103662, https://doi.org/10.1016/j.advwatres.2020.103662, 2020.

Tian, Y., Peters-Lidard, C. D., Eylander, J. B., Joyce, R. J., Huffman, G. J., Adler, R. F., Hsu, K., Turk, F. J., Garcia, M., and Zeng, J.: Component analysis of errors in satellite-based precipitation estimates, Journal of Geophysical Research, 114(D24), https://doi.org/10.1029/2009JD011949, 2009.

Troin, M., Arsenault, R., Wood, A. W., Brissette, F., and Martel, J. L.: Generating Ensemble Streamflow Forecasts: A Review of Methods and Approaches Over the Past 40 Years, Water Resources Research, 57(7), https://doi.org/10.1029/2020WR028392, 2021.

Tsai, W., Feng, D., Pan, M., Beck, H., Lawson, K., Yang, Y., Liu, J., and Shen, C.: From calibration to parameter learning: Harnessing the scaling effects of big data in geoscientific modelling, Nature Communications, 12(1), 1-13, https://doi.org/10.1038/s41467-021-26107-z, 2021.

Tyralis, H., and Papacharalampous, G.: Quantile-based hydrological modelling, Water, 13(23), 3420, https://doi.org/10.3390/w13233420, 2021.

Tyralis, H., Papacharalampous, G., Burnetas, A., and Langousis, A.: Hydrological post-processing using stacked generalization of quantile regression algorithms: Large-scale application over CONUS, Journal of Hydrology, 577, 123957, https://doi.org/10.1016/j.jhydrol.2019.123957, 2019.

Wang, Q. J., Robertson, D. E., and Chiew, F. H. S.: A Bayesian joint probability modeling approach for seasonal forecasting of streamflows at multiple sites, Water Resources Research, 45(5), W05407, https://doi.org/10.1029/2008WR007355, 2009.

Wu, J., Yen, H., Arnold, J. G., Yang, Y. C. E., Cai, X., White, M. J., Santhi, C., Miao, C., and Srinivasan, R.: Development of reservoir operation functions in SWAT+ for national environmental assessments, Journal of Hydrology, 583, 124556, https://doi.org/10.1016/j.jhydrol.2020.124556, 2020.

Xia, J.: Identification of a constrained nonlinear hydrological system described by Volterra Functional Series, Water Resources Research, 27(9), 2415-2420, https://doi.org/10.1029/91WR01364, 1991.

Xia, J., Wang, G., Tan, G., Ye, A., and Huang, G. H.: Development of distributed time-variant gain model for nonlinear hydrological systems, Science in China Series D: Earth Sciences, 48(6), 713-723, https://doi.org/10.1360/03yd0183, 2005.

Xu, L., Chen, N., Moradkhani, H., Zhang, X., and Hu, C.: Improving Global Monthly and Daily Precipitation Estimation by Fusing Gauge Observations, Remote Sensing, and Reanalysis Data Sets, Water Resources Research, 56(3), https://doi.org/10.1029/2019WR026444, 2020.

Yang, Q., Wang, Q. J., and Hakala, K.: Achieving effective calibration of precipitation forecasts over a continental scale, Journal of Hydrology: Regional Studies, 35, 100818, https://doi.org/10.1016/j.ejrh.2021.100818, 2021.

Ye, A., Duan, Q., Schaake, J., Xu, J., Deng, X., Di, Z., Miao, C., and Gong, W.: Post-processing of ensemble forecasts in low-flow period, Hydrological Processes, 29(10), 2438-2453, https://doi.org/10.1002/hyp.10374, 2015.

Ye, A., Duan, Q., Yuan, X., Wood, E. F., and Schaake, J.: Hydrologic post-processing of MOPEX streamflow simulations, Journal of Hydrology, 508, 147-156, https://doi.org/10.1016/j.jhydrol.2013.10.055, 2014.

Ye, A., Duan, Q., Zeng, H., Li, L., and Wang, C.: A distributed time-variant gain hydrological model based on remote sensing, Journal of Resources and Ecology, 1(3), 222-230, https://doi.org/10.3969/j.issn.1674-764x.2010.03.005, 2010.

Ye, A., Duan, Q., Zhan, C., Liu, Z., and Mao, Y.: Improving kinematic wave routing scheme in Community Land Model, Hydrology Research, 44(5), 886-903, https://doi.org/10.2166/nh.2012.145, 2013.

Yilmaz, K. K., Gupta, H. V., and Wagener, T.: A process-based diagnostic approach to model evaluation: Application to the NWS distributed hydrologic model, Water Resources Research, 44(9), W09417, https://doi.org/10.1029/2007WR006716, 2008.

Zhang, X., Liu, P., Cheng, L., Liu, Z., and Zhao, Y, A back-fitting algorithm to improve real-time flood forecasting, Journal of Hydrology, 562, 140-150, https://doi.org/10.1016/j.jhydrol.2018.04.051, 2018.

Zhang, Y., and Ye, A.: Machine Learning for Precipitation Forecasts Postprocessing: Multimodel Comparison and Experimental Investigation, Journal of Hydrometeorology, 22(11), 3065-3085, https://doi.org/10.1175/JHM-D-21-0096.1, 2021.

Zhang, Y., Ye, A., Nguyen, P., Analui, B., Sorooshian, S., and Hsu, K.: New insights into error decomposition for precipitation products, Geophysical Research Letters, 48(17), e2021GL094092, https://doi.org/10.1029/2021GL094092, 2021a.

Zhang, Y., Ye, A., Nguyen, P., Analui, B., Sorooshian, S., and Hsu, K.: Error Characteristics and Scale Dependence of Current Satellite Precipitation Estimates Products in Hydrological Modeling, Remote Sensing, 13(16), 3061, https://doi.org/10.3390/rs13163061, 2021b.

Zhang, Y., Ye, A., Nguyen, P., Analui, B., Sorooshian, S., and Hsu, K.: QRF4P-NRT Probabilistic Post-processing of Near-real-time Satellite Precipitation Estimates using Quantile Regression Forests, Water Resources Research, 58(5), e2022WR032117, https://doi.org/10.1029/2022WR032117, 2022a.

Zhang, Y., Ye, A., Nguyen, P., Analui, B., Sorooshian, S., and Hsu, K.: Dataset and results for "Comparing machine learning and deep learning models for probabilistic post-processing of satellite precipitation-driven streamflow simulation" [Data set]. Zenodo. https://doi.org/10.5281/zenodo.7187505, 2022b.

Zhao, L., Duan, Q., Schaake, J., Ye, A., and Xia, J.: A hydrologic post-processor for ensemble streamflow predictions, Advances in geosciences, 29(29), 51-59, https://doi.org/10.5194/adgeo-29-51-2011, 2011.

Zhao, P., Wang, Q. J., Wu, W., and Yang, Q.: Extending a joint probability modeling approach for post-processing ensemble precipitation forecasts from numerical weather prediction models, Journal of Hydrology, 605, 127285, https://doi.org/10.1016/j.jhydrol.2021.127285, 2022.

Zhou, X., Polcher, J., and Dumas, P.: Representing Human Water Management in a Land Surface Model Using a Supply/Demand Approach, Water Resources Research, 57(4), https://doi.org/10.1029/2020WR028133, 2021.

Zhu, S., Luo, X., Yuan, X., and Xu, Z.: An improved long short-term memory network for streamflow forecasting in the upper Yangtze River, Stochastic Environmental Research and Risk Assessment, 34(9), 1313-1329, https://doi.org/10.1007/s00477-020-01766-4, 2020.

https://doi.org/10.5194/hess-2022-377
Preprint. Discussion started: 21 November 2022
© Author(s) 2022. CC BY 4.0 License.

Zounemat-Kermani, M., Batelaan, O., Fadaee, M., and Hinkelmann, R: Ensemble machine learning paradigms in hydrology: A review, Journal of Hydrology, 598, 126266, https://doi.org/10.1016/j.jhydrol.2021.126266, 2021.